Review

Cobalt-catalyzed sulfate radical-based advanced oxidation: A review on heterogeneous catalysts and applications

Peidong Hu, Mingce Long*

School of Environmental Science and Engineering, Shanghai Jiao Tong University, 800 Dong Chuan Road, Shanghai 200240, People's Republic of China

ARTICLE INFO

ABSTRACT

Recently sulfate radical-based advanced oxidation processes (SR-AOPs) attract increasing attention due to their capability and adaptability in decontamination. The couple of cobalt and peroxymonosulfate (PMS) is an efficient way to produce reactive sulfate radicals. This article reviews the state-of-the-art progress on various heterogeneous cobalt-based catalysts for PMS activation, including cobalt oxides, cobalt-ferrite and supported cobalt by diverse substrates. We summarize the intrinsic properties of these catalysts and their fundamental behaviors in PMS activation, as well as synthetic approaches. In addition, influencing factors and synergistic techniques of Co/PMS systems in organic degradation and possible environmental applications are also discussed. Finally, we propose perspectives on challenges related to cobalt-based catalysts, heterogeneous Co/PMS systems and their potential applications in practical environmental cleanup.

© 2015 Elsevier B.V. All rights reserved.

Contents

* Corresponding author.
  E-mail address: long_mc@sjtu.edu.cn (M. Long).

1. Introduction

Organic contaminants in water remains being a great concern to the environment, especially those refractory and/or non-biodegradable pollutants that can hardly be treated by conventional methods. In recent decades, advanced oxidation processes (AOPs), which involve highly reactive oxygen species like hydroxyl radical ($^\bullet$OH), have attracted increasing attention due to their potential capability in the removal of recalcitrant organic pollutants. Upon such strong oxidants, organic pollutants are destructed into innocuous or low toxic small compounds, or even thoroughly mineralized into carbon dioxide and water [1,2]. As typical $^\bullet$OH-generating AOPs, Fenton reaction and its derivative technologies, such as photo-Fenton [3], electro-Fenton [4,5], sono-Fenton [6] and sono-photo-Fenton [7,8], are most popular due to the production of strong oxidant $^\bullet$OH (oxidation potential is 1.8–2.7 V vs. normal hydrogen electrode (NHE)) [9]. However, these methods keep facing several drawbacks, including massive utilization of ferrous salts and H_2O_2, chemical instability and difficulties in the storage and transport of the oxidant, low optimal reaction pHs (2–4), and subsequent separation and post-processing of huge amounts of sludge [10–13].

Advanced oxidation processes based on sulfate radical ($SO_4^{\bullet-}$) (SR-AOPs) have become to be a promising alternative owing to a series of merits that do not share with those $^\bullet$OH-generating methods: (a) $SO_4^{\bullet-}$ possesses an oxidation potential (2.5–3.1 V vs. NHE) comparable or even higher than $^\bullet$OH [14]; (b) $SO_4^{\bullet-}$ reacts more selectively and efficiently via electron transfer with organic compounds that contain unsaturated bonds or aromatic π electrons, while $^\bullet$OH may also react with diverse background constitutes by hydrogen abstraction or electrophilic addition at high reaction rates [14–16]; (c) $SO_4^{\bullet-}$, as a dominant oxidizing species, would react efficiently with organic compounds over a wide pH range of 2–8 [17–19]; (d) The half-life period of $SO_4^{\bullet-}$ is generally supposed to be 30–40 μs, which enables $SO_4^{\bullet-}$ to have more stable mass transfer and better contact with target compounds than $^\bullet$OH (less than 1 μs) [20–22].

$SO_4^{\bullet-}$ can be produced by radiolysis, photolysis, pyrolysis or chemical activation of peroxymonosulfate (PMS, HSO_5^-) or persulfate (PS, $S_2O_8^{2-}$) [23–27]. The oxidation potential of PMS (1.82 V) is higher than H_2O_2 (1.76 V) but lower than PS (2.01 V) [28]. However, PMS displays a more efficient performance in organic degradation processes [29]. Oxone, a commercial name of potassium peroxymonosulfate ($2KHSO_5 \cdot KHSO_4 \cdot K_2SO_4$), is a versatile and environmental friendly oxidant that has been widely utilized for bleaching, cleaning and disinfection and more importantly as a favorable source of PMS [30–32]. In fact, PMS can be activated by various transition metallic ions, such as Mn^{2+}, Ce^{3+}, Ni^{2+}, Fe^{2+}, V^{3+}, Ru^{3+} and so forth. Among them, the Co^{2+}/PMS system demonstrates the best performance that is even superior to traditional Fenton reaction at neutral pHs and with lower dosage of reagents [33,34].

Since catalytic decomposition of PMS using cobalt was first reported in 1958 [35], Co^{2+}/PMS system has successfully applied in chemiluminescent reactions [36,37], determination of trace Co^{2+} and PMS in aqueous solutions [38,39], modification of DNA [40] and SR-AOPs [30,41–43]. Cobalt-mediated activation of PMS can be illustrated as Fig. 1 [44]. It is apparent that the formation of $CoOH^+$, which is regarded as the most effective species to activate PMS (Eq. (1)), is the rate-limiting step [45,46], while the regeneration of Co^{2+} by reducing from Co^{3+} (Eq. (2)) is the crucial step to maintain the reactions at a low dosage of cobalt [47,48].
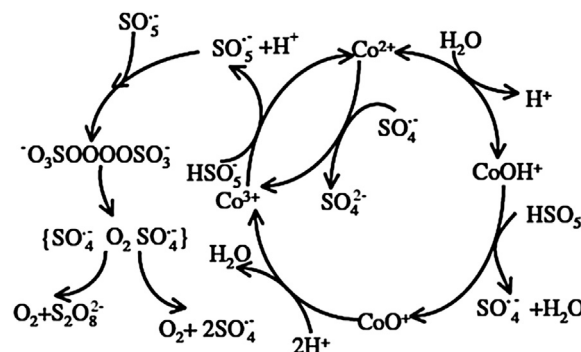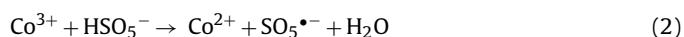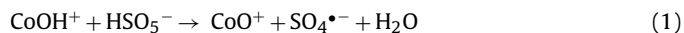
$$CoOH^+ + HSO_5^- \rightarrow CoO^+ + SO_4^{\bullet-} + H_2O \qquad (1)$$

$$Co^{3+} + HSO_5^- \rightarrow Co^{2+} + SO_5^{\bullet-} + H_2O \qquad (2)$$

Fig. 1. Mechanism on $SO_4^{\bullet-}$ chain reactions.
Source: Reproduced with permission from Ref. [31].

The average cobalt concentration in serum and urine of people are approximately 0.1–0.3 μg L^{-1} and 0.1 μg L^{-1}, respectively [49]. Although cobalt is claimed not being a hazardous chemical, several researches showed that excessive cobalt ions are possibly toxic and carcinogenic, leading to serious health problems such as asthma, pneumonia and cardiomyopathy [48,50,51]. Homogeneous catalytic reactions of Co^{2+}/PMS system in aqueous solutions discharge cobalt ions containing water, which is a potential threat to human beings and increases the operation cost due to the loss of cobalt. PMS activation using cobalt containing materials as heterogeneous catalysts (Co/PMS) seems to be a promising strategy. Multifarious heterogeneous cobalt-based catalysts have been investigated so far, including cobalt oxides, spinel-type ferrite particles and immobilized cobalt catalysts [51–58]. This review aims to provide a latest summary of various heterogeneous cobalt-based catalysts for PMS activation and their synthetic strategies. The influencing factors in the decontamination reactions, advanced techniques of synergistic heterogeneous Co/PMS systems and possible environmental applications will also be introduced. Challenges confronted in the application of Co/PMS are discussed in the conclusion and outlook section.

2. Heterogeneous catalysts

2.1. Cobalt oxide

Cobalt oxide is versatile in various industrial sectors, such as rechargeable batteries [59], air pollution control [60], Fischer–Tropsch synthesis [61] and gas sensors [62]. Up to now five cobalt oxides, CoO, CoO_2, Co_2O_3, CoO(OH) and Co_3O_4, have been reported. Among these species, CoO and Co_3O_4 are more frequently investigated while CoO_2 are thermally unstable [63–65]. Dionysiou's group first studied the heterogeneous activation of PMS by CoO or Co_3O_4 [66]. It was found that CoO/PMS system was inclined to be homogeneous because of significant dissolution of Co, which was attributed to the high solubility of CoO in water (0.313 mg/100 g H_2O) [49]. Chan et al. have found that even the filtrate of CoO possesses the ability to activate PMS [54]. However, in the form of Co_3O_4, the leakage of cobalt ions is much suppressed due to the bound of CoO in the net of Co_2O_3 [66]. Yu et al. have proposed the mechanism of Co_3O_4/PMS system, in which Co^{2+} ions are produced and participate in homogeneous redox reactions (Fig. 1), then Co^{3+} ions precipitate back into the crystal lattice of Co_3O_4, so as to decrease the loss of cobalt [67]. As the relatively higher stability, Co_3O_4 based SR-AOPs have been extensively investigated.

Plentiful methods have been applied to synthesize Co_3O_4 nanoparticles, such as thermal decomposition [68], polymer combustion [69], hydrothermal treatment [70,71], and sol–gel synthesis [72]. Among them, direct thermal decomposition of inorganic
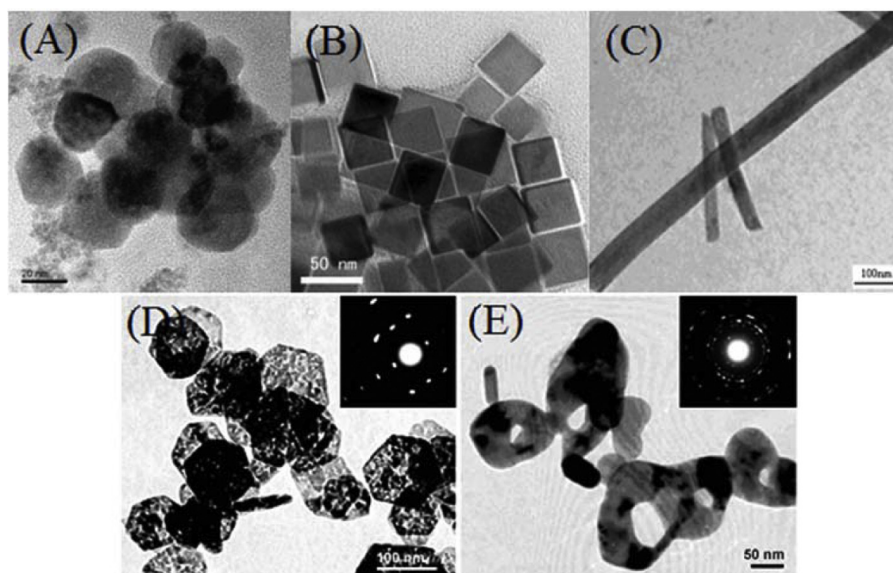
Fig. 2. Transmission electron microscope (TEM) images of various morphologies of nano-Co_3O_4: (A) nanospheres; (B) nanocubes; (C) nanorods; (D) nanosheets; (E) nanorings. *Source*: Reproduced with permission from Refs. [24,71,82,83].

or organometallic cobalt precursors, such as cobalt nitrate ($Co(NO_3)_2 \cdot 6H_2O$) [73], cobalt sulphate ($CoSO_4 \cdot 7H_2O$) [74], cobalt acetate ($Co(CH_3COO)_2 \cdot 4H_2O$) [75], cobalt oxalate ($CoC_2O_4 \cdot 2H_2O$) [76], is a facile and efficient way [77]. However, the products obtained from this method are usually a mixture due to the incomplete decomposition or phase transformation between Co_3O_4 and CoO, and exhibit uncontrollable size distribution or morphology [64,65]. Recently, other facile and effective synthetic strategies are developed to fabricate Co_3O_4 nanoparticles. Yang et al. have proposed a simple and low cost mechanochemical process [78]. According to this method, the precursor of Co_3O_4, $Co_2(OH)_2CO_3$ can be obtained on a large scale through a solid-state displacement chemical reaction by milling $Co(NO_3)_2 \cdot 6H_2O$ and NH_4HCO_3 in an agate mortar [78,79]. Molten salt synthesis (MSS) is a simple and environmental friendly process to prepare one-dimensional metal oxides without involving high pressures or surfactants. Through this method, Ke et al. synthesized Co_3O_4 nanorods that grew along an unusual $(-1, -1, 15)$ direction, which can be explained by the Ostwald ripening mechanism where molten ions (Na^+, K^+ and Cl^-) have a strong electrostatic interaction with the $(1 1 1)$ plane of Co_3O_4 nanocrystals [80]. A γ-ray irradiation redox route was proposed for the syntheses of Co_3O_4 nanoparticles at ambient conditions. The reactions do not require any reducing reagent, because of the generation of active reductants such as hydrated electrons and hydrogen atoms, which have reduction potentials even strong enough to reduce metal oxides to metal atoms [81].

It is clear that the activity of different Co_3O_4 facets that interacts with other substances, such as O_2, H_2O, CO and heavy metals, is discrepant due to different geometric and electronic structures [84–87]. The performance of Co_3O_4 in heterogeneous catalysis, like SR-AOPs, could also depend much on their morphologies and structures (Fig. 2). Hydrothermal method is frequently employed to synthesize Co_3O_4 nanoparticles or their precursors with tunable morphologies. Liu et al. have synthesized single-crystalline hexagonal β-$Co(OH)_2$ nanosheets through hydrothermally treating the cobalt nitrate using trimethylamine as both alkaline and complexing reagent [83]. Porous Co_3O_4 nanosheets and nanorings were obtained by calcining the precursor β-$Co(OH)_2$ at 400 °C and 600 °C, respectively. Chao et al. reported a one-pot hydrothermal method to prepare Co_3O_4 nanocubes in the presence of sodium dodecyl benzene sulfonate (SDBS),

and subsequent calcinations were not required because final spinel Co_3O_4 nanocubes were obtained directly from $Co(OH)_2$ at a relatively lower hydrothermal temperature (160 °C) [71]. Microwave-assisted hydrothermal (MAH) method is another popular technique due to the advantages of high energy efficiency, short reaction time, low cost and high reproducibility [82,88,89]. The movement and polarization of ions in the aqueous solution under the rapidly changing microwave electric field will result in transient anisotropic microdomains in the reaction system, and make it possible to separate the nucleation and growth of nanocrystals [90,91]. Through adjusting the reaction parameters such as reaction time, temperature, precursors, and surfactants during the MAH method, the precursors of Co_3O_4, like $Co_2(OH)_2CO_3$, CoC_2O_4 and $Co(OH)_2$, with diverse morphologies, including nanocubes, nanorods and nanoflakes, can be synthesized [52,82,90–92]. Surfactants and ligands, like trioctylphospine, triphenylphospine, hexadecyltrimethylammonium bromide (CTAB), polyacrylamide, oleylamine and trimethylamine, are preferable to be employed to control crystal growth. These additives binding to the metal nanoparticles serve as soft colloidal templates and provide steric hindrance, which can not only slow down the growth of nanoparticles, but also result in specific nanostructures [93–97]. Moreover, relative growth rates along different orientations can be modified by surfactants or inorganic additives due to their preferential adsorption [98,99]. For example, CTAB plays an important role in the control of linear dimensional growth of cobalt oxalate in a microemulsion method [100], while the carbonate anions (CO_3^{2-}) selectively inhibit the growth along both $(0 0 1)$ and $(1 0 0)$ directions of cobalt hydroxyl carbonate during the process of precipitation [101]. The initial concentration of cobalt source also influences the morphologies of Co_3O_4 [71,102]. The products of nanoplates, semi-convex superstructures or microspheres were synthesized through a polyol process with the increase of initial concentration of cobalt acetate [102].

2.2. Cobalt-ferrite

Spinel cobalt-ferrite ($CoFe_2O_4$) is an excellent electrical and magnetic material with high coercivity and moderate magnetization. It has been widely applied in high frequency electronics [103], microwave devices [104], high density magnetic recording
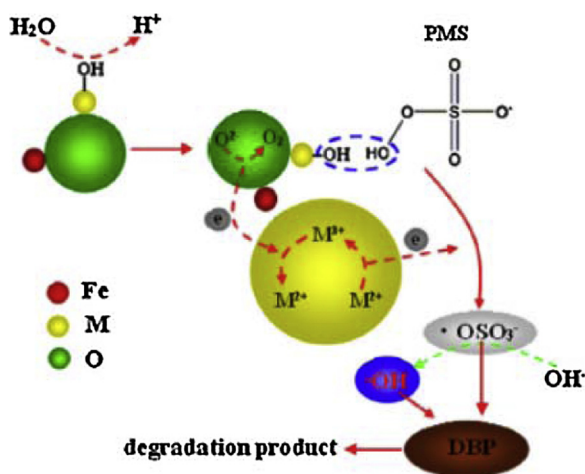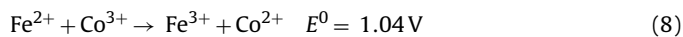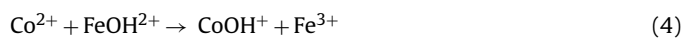
Fig. 3. Activation mechanism of MFe_2O_4 (M = Co) inducing PMS. *Source*: Reproduced with permission from Ref. [55].

[105], ferrofluids [106], and hyperthermia based tumor treatment [107,108]. $CoFe_2O_4$ is superior to Co_3O_4 in PMS activation, including: (a) the cobalt in $CoFe_2O_4$ is divalent, while Co(III) in Co_3O_4 shows some detrimental effects on PMS activation [109]; (b) $CoFe_2O_4$ can markedly suppress cobalt leaching due to strong Fe–Co interactions [56,110]; and (c) $CoFe_2O_4$ is easier to be separated from reaction system by an external magnetic field due to its unique ferromagnetic behavior [55,111]. In addition, the presence of Fe is found to be beneficial for enriching hydroxyl groups and $CoOH^+$ on the surface of Fe–Co catalysts (Eqs. (3) and (4)), and the formation of $CoOH^+$ is a vital step to activate PMS (Eq. (1)). Fig. 3 describes the processes of PMS activation by $CoFe_2O_4$. Metal ions serve as Lewis acid and capture H_2O to form activated hydroxyls on the surface of $CoFe_2O_4$, and simultaneously HSO_5^- is bonded in the form of $CoFe_2O_4$-O-H-HSO_5^- through hydrogen bonds. Then Co^{2+} ions transfer electrons to break the O—H and O—O bonds and be oxidized to Co^{3+}, accompanying with the generation of $SO_4^{\bullet-}$ radicals. Meanwhile, the lattice oxygen is oxidized to O_2 during the process of reduction of Co^{3+} (Eqs. (2) and (5)). On the other hand, O_2 in the solution would replenish the oxygen-deficient surface to maintain the activity of catalysts. The balance among Co^{2+}/Co^{3+}, O^{2-}/O_2 and PMS was thought to be critical for the high efficiency of catalytic decontamination. According to the standard reduction potentials (Eqs. (6) and (7)), catalysts containing both Fe and Co would promote the regeneration of Co^{2+} [56]. The reduction of Co^{3+} by Fe^{2+} is thermodynamically favorable (Eq. (8)).

$$Fe^{3+} + H_2O \rightarrow FeOH^{2+} + H^+ \tag{3}$$

$$Co^{2+} + FeOH^{2+} \rightarrow CoOH^+ + Fe^{3+} \tag{4}$$

$$SO_5^{\bullet-} + O^{2-} \rightarrow SO_4^{\bullet-} + O_2 \tag{5}$$

$$Fe^{3+} + e^- \rightarrow Fe^{2+} \quad E^0 = 0.77\,V \tag{6}$$

$$Co^{3+} + e^- \rightarrow Co^{2+} \quad E^0 = 1.81\,V \tag{7}$$

$$Fe^{2+} + Co^{3+} \rightarrow Fe^{3+} + Co^{2+} \quad E^0 = 1.04\,V \tag{8}$$

Various techniques have been developed to synthesis highly efficient $CoFe_2O_4$ nanoparticles. In a typical sol–gel procedure, aqueous solution of cobalt salt and ferric salt are dropwise added into a solution with additives, like citric acid, sodium dodecyl sulfate (SDS) or even egg white, and a brown gel is formed by evaporating the mixture in a water bath, and finally $CoFe_2O_4$ nanoparticles are obtained by calcination [55,112,113]. Additive surfactants can not only prevent aggregation of primary particles during the synthesis, but also be a fundamental driving force to the self-assembling of the primary nanoparticles of spherical

aggregates with a high surface area [113]. Generally, amorphous phase of $CoFe_2O_4$ is obtained at low calcination temperatures, while highly crystallized $CoFe_2O_4$ with decreased specific surface areas is achieved at high calcination temperatures due to the coalescence of crystallites, both of which would significantly limit PMS activation [112,114].

Co-precipitation method is another frequently applied method. According to this method, $CoFe_2O_4$ can be obtained directly by adding sodium hydroxide into previously prepared mixture solution of cobalt salt and ferric salt without further processing [111]. Kuruva et al. pointed out that the increase of co-precipitation pH and calcination temperatures would result in a simultaneous increase of lattice constants and average particle sizes, and helpful in minimizing the polydispersity in synthesized $CoFe_2O_4$ [115]. In order to restrict the particle growth and decrease the particle sizes, capping agents, like ricin oil, are added into the bimetallic solution before the addition of alkaline solution [116]. The combination of co-precipitation and mechanochemical treatment is another way to prepare $CoFe_2O_4$ without surfactants [117]. Yang et al. applied the mechanochemical method to the precipitates using NaCl as the diluent [118]. The results indicated that this method inhibited the agglomeration and facilitated the crystallization of $CoFe_2O_4$ nanoparticles. Senapati et al. also developed a surfactant-free co-precipitation method by combining with the sonochemical technique [119]. All solutions in the process were placed in an ultrasonic bath, and products were directly received after repetitive ultrasonic irradiation. During ultrasonic irradiation, cavitation effects create high pressure and temperature to induce in situ calcinations, and $CoFe_2O_4$ can be directly obtained without further thermal treatment. Moreover, according to this method, excessive hydroxyl ions are entrapped to form basic sites, which are responsible for excellent stable dispersion of $CoFe_2O_4$ nanoparticles in polar protic solvent, like aqueous or alcoholic medium.

In general, solvo(hydro)thermal methods provide many advantages over other methods, including simplicity, the high crystallinity of products, relatively low synthetic temperatures and the possibility of tunable crystal growth [120]. Generally, hydrothermal syntheses involve a combination of co-precipitation and hydrothermal treatment. Pervaiz et al. successfully prepared one-dimensional $CoFe_2O_4$ nanorods through a hydrothermal way at $160\,^\circ C$ using CTAB as the surfactant [103]. CTAB was not only responsible for the assembly of rod nanoparticles, but also produced the crystal growth initializers by the electrostatic interaction between CTA^+ cationic ion and the negatively charged Fe-OH-Co. By adjusting the stoichiometric Fe/Co ratio, Su et al. synthesized a series of $Co_xFe_{3-x}O_4$ (x = 0, 0.2, 0.5, 0.75) magnetic nanoparticles using a hydrothermal method [56]. The results showed that the decomposition rate of Rhodamine B (RhB) increased with the increase of cobalt contents in the magnetite catalysts, which were attributed to not only the higher activation rate of HSO_5^- caused by the doping cobalt species, but also the strong intimate Fe-Co interactions to form $CoOH^+$ (Eqs. (3) and (4)). In solvothermal synthesis, organic solvents can dissolve reactants to form solvent-reactant complex and affect the concentration and state of active species, which will change the reaction rates and processes [121]. Yanez-Vilar et al. reported a modified approach that the solvent, benzyl alcohol or hexanol, was used as both a solvent and a ligand [120]. It was found that the $CoFe_2O_4$ nanoparticles produced using hexanol were slightly smaller than benzyl alcohol, because the higher Lewis basicity of hexanol enhanced the solvolysis of the acetylacetonate.

2.3. Supported cobalt catalysts

Besides directly using the cobalt compounds for PMS activation, the catalysts can also be immobilized cobalt species on various materials. The supported cobalt catalysts exhibit significantly

suppressed leakage of cobalt ions, and can also lead to higher catalytic activity and stability due to the novel physicochemical properties originated from the interaction between cobalt species and supporters [122–125].

Generally, supported cobalt catalysts can be synthesized through various approaches, including impregnation [46], sol–gel [126], hydrothermal [127], co-condensation [128], and solution combustion synthesis [125]. Among these methods, impregnation is an extensively applied facile way. According to this method, support materials are immersed in a solution containing active species, like cobalt ions, and the suspension is stirred until these active species immobilized on the surface or in the pores of the supports, then the catalysts can be obtained after drying and calcinations. Surface modification of the support in a pretreatment process can facilitate the binding or complexation of other metal ions or groups. According to Chen et al., when majority of sodium cations on the surface of the titanate nanowires (TNWs) were replaced by protons, higher density cobalt ions would adsorb on TNWs [129]. In addition, the precursors of cobalt play an important role in the stability and efficiency of the supported catalysts. The precursors of $CoCl_2$, $Co(NO_3)_2$, $Co(CH_3COO)_2$ and $CoSO_4$ have been investigated [53,128,130,131]. The residual Cl^-, CH_3COO^- and SO_4^{2-} can not only cover cobalt species but also substantially weaken the metal-support interaction, and the removal of them requires thermal treatment at a high temperature (>500 °C). However, catalysts prepared from $Co(NO_3)_2$ demonstrate a strong metal-support interaction, resulting in smaller sizes and better dispersions of Co_3O_4 crystalline. The catalysts would be free of NO_3^- after being thermally treated below 500 °C [53,130]. The stability of TiO_2 or SiO_2 (SBA-15) supported cobalt catalysts prepared by different cobalt precursors followed the order: $Co(NO_3)_2 > Co(CH_3COO)_2 > CoCl_2 > CoSO_4$, while the efficiency of degradation of organic compounds followed a reverse order, which was attributed to the homogeneous reactions by the significantly leached cobalt ions [53,128,130].
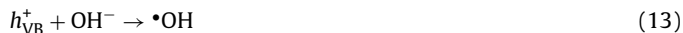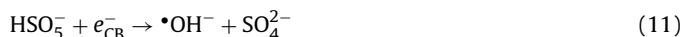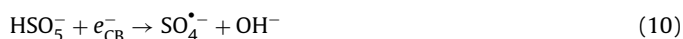
Solution combustion synthesis (SCS), characterized as highly exothermic, self-sustained, energy-saving and effective, is suitable for producing a variety of high-surface area powders and nanoscale catalysts [125,132]. In a typical one-step SCS method for supported cobalt catalysts, a cobalt salt (generally nitrate) is dissolved with a fuel compound, like urea, glycine or citric acid, and stirred with supports, and then the mixture is put in a preheated oven at a given temperature for auto-ignition [125,133]. The chemical composition of the products can be simply tuned by varying the precursors (metal salt and fuel) [134]. Catalysts prepared from glycine contain more defective structures because of the high velocity of combustion front propagation, and are more active for phenol degradation in the presence of PMS [125,135].

2.3.1. Oxide supports

Oxides, such as TiO_2, MgO, Al_2O_3, SiO_2, MnO_2 and ZnO, have been extensively investigated as the support for catalytic applications. It was reported that the acidity of oxides follows the order of $SiO_2 > Al_2O_3 > TiO_2 > MgO$ [133,136]. Since cobalt ions can be regarded as Lewis acid, the presence of basic centers on the support surface favors the dispersion of cobalt species, which would increase the contact between cobalt species and PMS and contribute to an improved catalytic efficiency. The better catalytic activities of cobalt immobilized TiO_2 and MgO are attributed to their basic character and the better dispersions of Co_3O_4 on their surface [133,137,138]. Moreover, Stoyanova et al. confirmed that cobalt oxides supported on materials with relatively acidic surface such as Al_2O_3 displayed a weaker catalytic activity compared with that of the MgO supported analogs [138]. Simultaneously, basic centers would result in a highly hydroxylated surface that facilitates the formation of $CoOH^+$, which is crucial for PMS activation

and consequently contributes to a more rapid oxidation reaction (Eq. (1)) [53,138]. Hu et al. have found that loading Mg into the support of SBA-15 generated remarkable basicity of the surface, which facilitated the dispersion of Co_3O_4 on the support, and promoted the formation of $CoOH^+$ [137]. Furthermore, the intimate interactions between cobalt and the surface of the supports, such as Co–Si and Co–Ti, can improve the stability of the catalysts and remarkably diminish the leakage of pernicious metallic ions [125,139]. In addition, some metal oxide supports, such as CuO [140], MnO_2 [141] or RuO_2 [142], can serve as catalysts for PMS activation by themselves. Therefore, loading cobalt species on such supports would display a synergistic effect that contributes to a stronger oxidization potential, faster $SO_4^{\bullet-}$ production and higher decontamination rate [143].

TiO_2 and ZnO are well-known environmental friendly semiconductor photocatalysts that work under the irradiation of ultraviolet (UV) light. Electrons in the valence band (VB) of pure TiO_2 and ZnO can only be excited by UV light to the conduction band (CB), leaving positive holes behind [144]. Loading cobalt on TiO_2 and ZnO would induce partial Co^{2+} ions doping into the lattice and forming impurity levels, so that the hybrids (e.g. Co_3O_4/TiO_2, $CoFe_2O_4/ZnO$) are capable of responding to visible (Vis) light (Fig. 4) [122,145]. Meanwhile, cobalt species immobilized on the surface of photocatalysts serve as active spots to activate PMS (Fig. 4B). In addition, the electron (hole) transfer between the cobalt ions and supports can reduce e_{CB}^-/h_{VB}^+ recombination. The photogenerated electrons help not only to regenerate Co^{2+} by reducing Co^{3+}, but also to activate PMS (Eqs. (9)–(11)), while VB holes are responsible for the oxidation of surface hydroxyls and adsorbed water molecules and the formation of another highly reactive radical $^\bullet OH$ (Eqs. (12) and (13)) [122,146]. It should be pointed out that holes are also directly engaged in the degradation of organic compounds due to their high oxidization ability. Therefore, Co/TiO_2 and Co/ZnO can be regarded as promising multi-functional catalysts in the Co/TiO_2 (ZnO)/PMS/UV–Vis heterogeneous hybrid systems [53,122,124,145–147].

$$Co^{3+} + e_{CB}^- \rightarrow Co^{2+} \tag{9}$$

$$HSO_5^- + e_{CB}^- \rightarrow SO_4^{\bullet-} + OH^- \tag{10}$$

$$HSO_5^- + e_{CB}^- \rightarrow {}^\bullet OH^- + SO_4^{2-} \tag{11}$$

$$h_{VB}^+ + H_2O \rightarrow {}^\bullet OH + H^+ \tag{12}$$

$$h_{VB}^+ + OH^- \rightarrow {}^\bullet OH \tag{13}$$

2.3.2. Molecular sieve supports

Zeolite, one of the most common molecular sieves that consists of a three-dimensional network of metal-oxygen tetrahedra (sometimes also octahedra), possesses many important properties, including the size and shape selectivity of microporous structures, the potential to have strong acidity, ion exchangeable sites and highly hydrothermal stability [148]. The connection of cations in the Si/Al framework of zeolites is weak, therefore metal ions in the supercages and channels of molecular sieves can be exchanged by ion exchange or impregnation in a dilute, neutral or slightly acidic solution. Acidic and basic solution should be avoided because of the side reactions of proton exchange and the production of hydroxides precipitation [50,149].

Cobalt containing zeolite has been successfully synthesized and used widely for various applications such as Fischer–Tropsch reactions [150], epoxidation of styrene [151], and adsorption of CO_2 [152]. Shukla et al. synthesized three different types of cobalt containing zeolites (A, X and ZSM-5) by an ion exchange method for PMS activation [50]. The results indicated that zeolite A and X lost crystallinity after cobalt ions exchange, and the serious leaching of
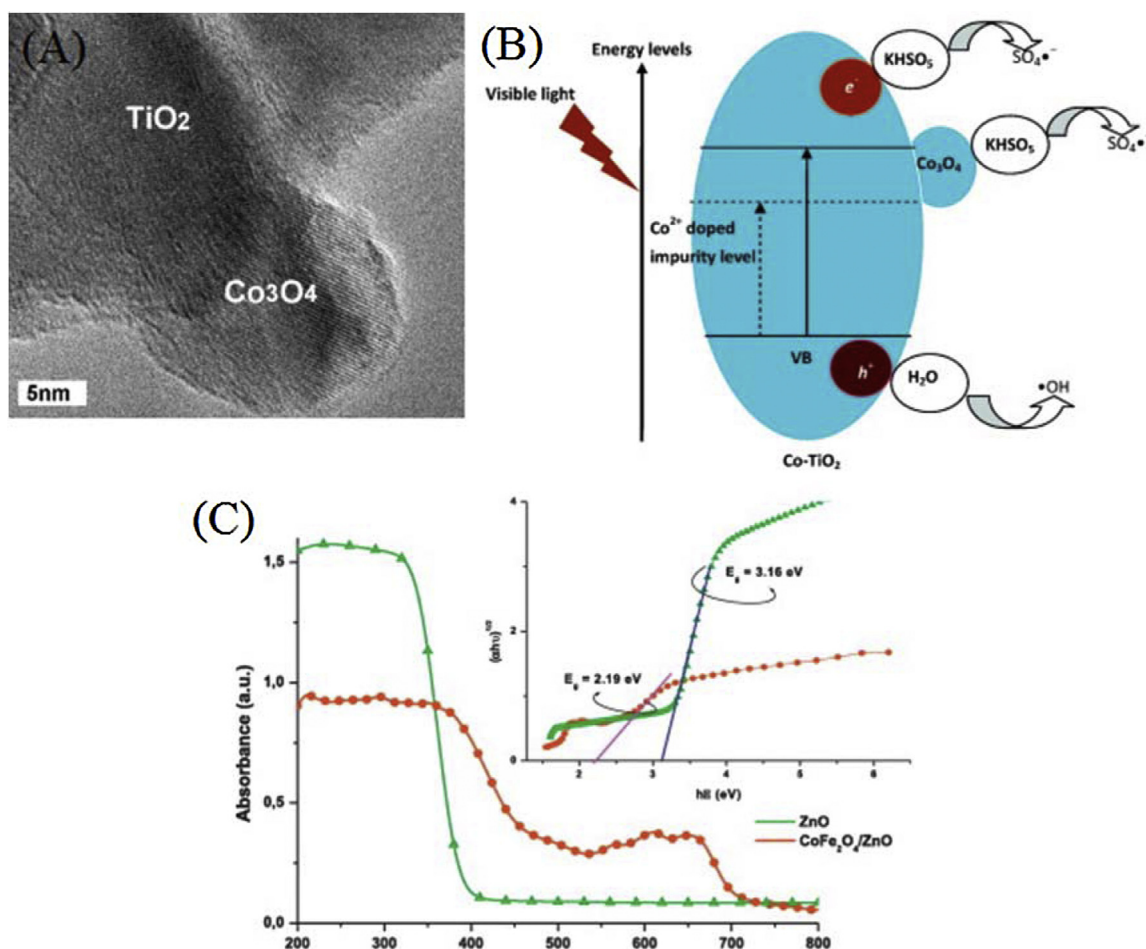
Fig. 4. (A) TEM image and (B) schematic representation of the band structure of Co_3O_4/TiO_2. (C) Diffuse reflectance spectrum of ZnO and $CoFe_2O_4/ZnO$ nanoparticles and inset shows Tauc plot for ZnO and $CoFe_2O_4/ZnO$ nanoparticles.
Source: Reproduced with permission from Refs. [46,122,145].

cobalt ions results in much faster reaction rates due to the homogeneous activation of PMS. However, ZSM-5 exhibited an undisturbed crystalline structure and a stable catalytic performance for phenol degradation. It was revealed that the Si/Al ratio in zeolites has a direct effect on the format of incorporated cobalt species [50,149,153]. Zeolite A and X are low-silica zeolites with the Si/Al ratio of 1 and 1.25, respectively, and the high density of AlO_4^- contributes to the dominant exchangeable Co^{2+} in the distort local lattice. Oppositely, ZSM-5 is a high-silica zeolite with a Si/Al ratio up to 50, and cobalt ions mainly turn into the oxide forms (Co_3O_4, CoO or $CoAl_2O_4$). Pierella et al. prepared Co_3O_4/ZSM-5 through calcining the as-prepared samples obtained by impregnating NH_4^+-ZSM-5 in a solution of cobalt chloride [154]. It was found that the Brönsted to Lewis acid sites ratio on the surface was apparently reduced in the presence of cobalt. However, the disappearance of Brönsted acidity was insignificant, indicating that a great amount of cobalt was not at exchangeable positions. As cheaper porous aluminosilicate materials, natural zeolites have also been used as the substrates for cobalt immobilization. Cobalt supported on Indonesian natural zeolite (Co/INZ) could achieve complete degradation of phenol in 5 h with the presence of PMS, even faster than Co/ZSM-5 under the same reaction conditions ($0.4\,g\,L^{-1}$ catalyst, $2\,g\,L^{-1}$ oxone, 25 ppm phenol and 25 °C) [50,148].

Molecule sieves with mesoporous structures are first reported by Kresge et al. in 1992 [155], which have highly ordered pores, narrow pore size distributions (2–50 nm) and large surface areas. SBA-15 and MCM-41, as typ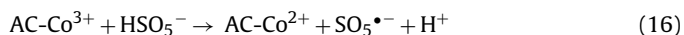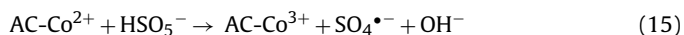ical silica mesoporous molecule sieves with two dimensional hexagonal arrays of uniform mesopores, have attracted much attention in the field of catalysis [156,157]. SBA-15 has better hydrothermal stability due to its thicker siloxane pore walls [158,159], while MCM-41 possesses a larger specific surface area (>1000 m^2/g) [160]. By chemical interactions between silanol groups and transition metal ions, cobalt and other metallic elements can be incorporated into the hexagonally arranged framework of silica, resulting in excellent catalytic activities [160–162]. Impregnation and ion exchange are common synthesis techniques. It was found that pore sizes of SBA-15 had an influence on the size and dispersion of immobilized metal oxides [163]. Metal oxides tend to aggregate and block the mesoporous interconnections in the silica with larger mesopores, which increases the diffusional resistance and weakens the catalytic activities. However, when pore size of the silica was relatively smaller, metal oxides with reduced crystal sizes would form in the residual micropores in the inorganic walls of the mesoporous structures. In addition, the solvent used for impregnation affected the dispersion of metal oxides (Co_3O_4), and a double-solvent technique was developed as an improvement strategy [164,165]. In this method, an alkane solvent, such as n-hexane, n-pentane, n-heptane or cyclohexane, was firstly applied as the prewetting agent to increase the number of germinal and hydrogen-bonded silanol and augment the hydrophilic nature of silica frameworks, which would favor the interaction between SBA-15 and the cobalt containing solution introduced afterward [166]. Among the alkane solvent, pentane was perfect due to the lower interfacial tension

between pentane and water, and the smaller droplets formed in pentane enhanced the dispersion of cobalt oxide nanoparticles on SBA-15. SBA-15 and MCM-41 supported catalysts can also be prepared by co-condensation method without destroying the mesoporous structures [128,161,167]. According to this method, cobalt precursors are mixed with a silica source and templates for co-condensation of cobalt and silica during mesoporous silica synthesis. Cobalt can be incorporated into the structure of silica rather than being simply attached on the surface, which significantly limits the leaching of cobalt ions. It was found that the incorporation of cobalt into the framework of MCM-41 exhibits a higher catalytic activity toward PMS activation than the surface loading cobalt oxides on MCM-41 in the removal of caffeine (CAF) [161].

2.3.3. Carbon derived supports

Carbon derived materials, such as activated carbon (AC), activated carbon fibers (ACFs), graphite, and recently emerging carbon nanotubes (CNTs), graphene (G), graphene oxide (GO), reduced graphene oxide (rGO) and carbon aerogels (CAs), etc., are regarded as promising supports due to their high specific surface area, controllable pore size, chemical inertness, conductivity and adsorption properties.

Activated carbon is an environmental friendly and economical adsorbent that has been widely used in the removal of organic contaminants from wastewater. Furthermore, it was revealed that AC itself could activate some oxidants, like H_2O_2, PS and PMS, to generate reactive radicals [168]. A possible reaction in the presence of AC and PMS showing as Eq. (14) [57]. When cobalt species are immobilized on AC, $SO_5^{\bullet-}$ and $SO_4^{\bullet-}$ can be generated at faster rates (Eqs. (15) and (16)), and organic compounds decomposition can be achieved in a short time. Unlike catalysts mentioned above, metal oxides anchored onto AC could be reduced during the treatment due to the reducibility of AC. Shukla et al. [57] found that the main cobalt oxides in Co/AC catalyst was Co_2O_3 instead of Co_3O_4, while Xu et al. [169] obtained a mixture of $CoFe_2O_4$ and Co_xFe_y by calcining the precursors containing Co, Fe and AC.

$$AC + HSO_5^- \rightarrow AC\text{-}H + SO_5^{\bullet-} \qquad (14)$$

$$AC\text{-}Co^{2+} + HSO_5^- \rightarrow AC\text{-}Co^{3+} + SO_4^{\bullet-} + OH^- \qquad (15)$$

$$AC\text{-}Co^{3+} + HSO_5^- \rightarrow AC\text{-}Co^{2+} + SO_5^{\bullet-} + H^+ \qquad (16)$$

Activated carbon fibers (ACFs) not only possess large surface areas with high adsorption capacity and unusual chemical stability, but also have plenty of active groups on the surface that ensure the stable immobilization and excellent dispersion of active species [170,171]. Combined with cobalt phthalocyanine (CoPc), ACFs-CoPc was proven to be an efficient heterogeneous catalyst for PMS activation to remove dyes, but the leaching of cobalt ions was nearly undetectable. This can be attributed to the strong chemical bonds formed between ACFs and functional groups in the phthalocyanine structure [171].

Graphene, a two-dimensional single layer of sp^2-hybridized carbon material, has attracted tremendous interest due to its ultra-large specific surface area, excellent electrical conductivity and extraordinary mechanical strength [172]. It is easier to obtain graphene oxide and reduced graphene oxide in a large scale through chemical exfoliation methods [173]. GO consists of a hexagonal ring-based carbon network with both sp^2- and sp^3-hybridized carbon atoms [174]. These carbon materials have multiple oxygen-containing functional groups, such as hydroxyls and epoxides in the basal plane, and carboxyl groups at plane edges [175], which make GO swell readily and disperse in water easily. These exfoliated GO sheets are potential supports to load various nanocrystals with excellent dispersions [176–179]. Several GO (rGO) supported cobalt catalysts, such as Co_3O_4/GO [45], $CoFe_2O_4$/rGO [180] and

$Co(OH)_2$/rGO [127], have been studied in SR-AOPs. The unexpected improvements of catalytic activity for PMS activation and the degradation of organic compounds were observed, in contrast to unsupported ones, suggesting a synergistic coupling between cobalt species and GO (rGO) [175,181]. The reasons for this synergistic effect can be briefly summarized as: (a) GO (rGO) has a peculiar electronic structure and plays an important role in electron transfer between cobalt species and PMS, facilitating the catalytic cycles as shown in Fig. 1 [180,182,183]; (b) the strong covalent bond interactions with Co_3O_4 (Co—O—C) contributes to the excellent dispersion of Co_3O_4 nanoparticles and favors the formation of $CoOH^+$ (Fig. 5) [182,184]; (c) rGO with a certain reductive degree could also serve as a catalyst to activate PMS when it possesses a proper amount of electron-rich groups (such as ketonic groups) or enriched defects as Lewis basic sites [185,186]; (d) their extraordinary adsorption capacity of GO (rGO) significantly promotes the target substance to accumulate on the catalyst surface and approach the active oxidants.

Recently, monolithic carbon aerogel (CA) or xerogel (CX), deriving from resorcinol formaldehyde resin (RF) [187], GO [188], biomaterials [189] and so forth, have also become a great hit in various applications due to their abundant connected hierarchical pores, large specific surface area, outstanding electrical conductivity and low mass density. Most importantly, these carbonaceous materials are macroscopic and can be prepared with desirable sizes and morphologies. As catalyst supports, they can be removed from the reaction system easily, and reused with a simple post-treatment [126]. Sun et al. prepared two Co/CX catalysts by either in situ cobalt ion doping (Co/CX-G) or impregnation (Co/CX-I), where CX was synthesized by a sol–gel method from resorcinol and furfural [190]. It was founded that Co/CX-I exhibited a higher adsorption and catalytic activity in the activation of PMS for phenol degradation than that of Co/CX-G, because impregnation favored the formation of smaller cobalt oxide particles while doped cobalt in CX prevented the formation of micropores and resulted in larger cobalt oxide particles.

2.3.4. Metal–organic frameworks

Metal–organic frameworks (MOFs), a kind of crystalline inorganic–organic hybrids, have been developed as an emerging porous material. They possess several advantages over conventional molecular sieves and carbon materials, including high thermal and chemical stability, large surface areas and high pore volumes. Till now, many MOFs based composites have been developed, such as MOF/metal oxide [191], MOF/silica [192], MOF/organic polymer [193], as well as MOF/carbon [194], and applied in gas adsorption/storage [195], chemical separation [196] and drug delivery [197]. Lin et al. directly applied a cobalt-based MOF, zeolitic imidazole framework (ZIF)-67, to activate PMS for RhB degradation [198]. The activation capacity of ZIF-67 was superior to conventional Co_3O_4 nanoparticles due to its high surface area and porosity. Zeng et al. have successfully synthesized yolk-shell Co_3O_4/MOFs by a one-pot solvothermal method in the absence of any templates (Fig. 6A), which were applicable for SR-AOPs [199]. The Co_3O_4/MOF nanocomposites contain a void cavity between Co_3O_4 core and uniform MOF-5 shell, and could be regarded as a nanoreactors where encapsulated Co_3O_4 nanoparticles steadily activate PMS to degrade 4-chlorophenol (4-CP) in a confined microspace (Fig. 6B and C). The mesoporous and adsorptive MOFs shells not only preserve the surface active sites of Co_3O_4, but also guarantee a rapid diffusion of reactants.

MOFs or MOF-hybrid composites can also be used as precursors to prepare carbonaceous or non-carbonaceous materials with hierarchical pore structures [200]. According to this strategy, Lin et al. prepared a magnetic Co_3O_4/GO (MCG) nanocomposite by simple calcination of products obtained from the electrostatic

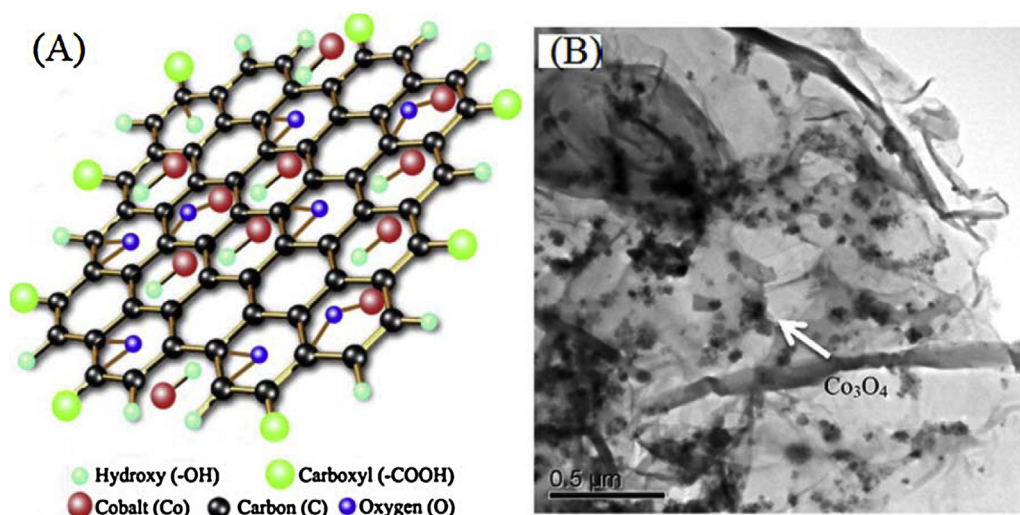**Fig. 5.** (A) Scheme and (B) TEM image of Co_3O_4/rGO.
Source: Reproduced with permission from Refs. [45,182].

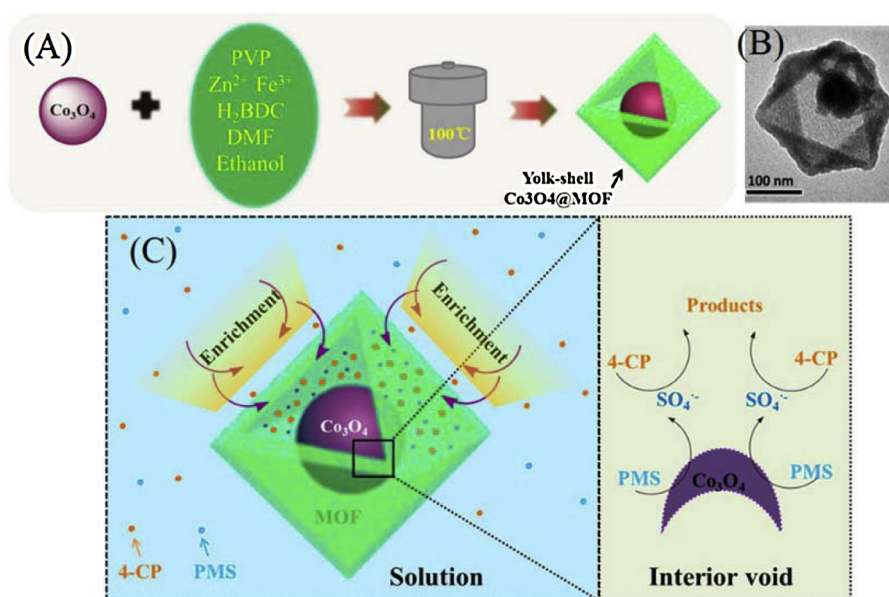**Fig. 6.** (A) Preparation procedure and (B) TEM image of Co_3O_4/MOFs, and (C) possible mechanism of 4-CP degradation.
Source: Reproduced with permission from Ref. [199].

self-assembly of ZIF-67 and GO [201]. MCG, consisting of porous Co_3O_4-bearing nanoparticles deriving from ZIF-67, could be a single sheet after dispersion in water, and possessed an enhanced catalytic performance owing to the interfacial interaction between carbonized ZIF-67 and rGO. On the other hand, Qin et al. innovatively synthesized magnetic $CoFe_2O_4$ nanocomposites using a Fe-containing MOF (MIL100-Fe) as both template and precursor [202]. $Co(NO_3)_2 \cdot 6H_2O$ was immobilized in the pores of MIL100-Fe by incipient wetness impregnation with different Fe/Co molar ratio. After thermal treatment, the as-prepared $CoFe_2O_4$ nanoparticles retained the morphology of MOF, and could remove approximately 95% of phenol in 2 h when using PMS as the oxidant.

2.3.5. Magnetic cobalt catalysts

Separation of nanocatalysts from aqueous solutions is a major problem for the practical application in water purification. As conventional separation methods, filtration would cause the blockage of filters, while centrifugation could hardly achieve thorough separation even with a high energy consumption. In recent decades,

magnetic catalysts have been regarded as an ideal solution to this problem due to its simplicity of separation by applying an external magnetic field. Fortunately, $CoFe_2O_4$ exhibits ferrimagnetism [203], and the hybrids, such as $CoFe_2O_4$/TiO_2 [147], $CoFe_2O_4$/Co_xFe_y/AC [169] and $CoFe_2O_4$/rGO [204], all possess the magnetically separable property, and can be easily recycled by the magnetic separation technique.

Fabricating core/shell structural magnetic catalysts is an important strategy to inhibit the aggregation of magnetic mediums, enhance the thermal and chemical stabilities, and allow conjugation of desirable molecules onto the surface [160,205–207]. Due to the chemical and physical stability, ferrimagnetic oxides (Fe_3O_4, α-FeOOH, $CuFe_2O_4$, γ-Fe_2O_3) are frequently used as the magnetic mediums, which can supply high saturation magnetization (M_s) and small coercive force (H_c) [160,169,208]. Wang et al. successfully synthesized a core/shell catalyst of magnetic carbon nanospheres (Fe_3O_4/CS) with cobalt oxide loading (Co/MCS) (Fig. 7A), and it was proven to be excellent for heterogeneous activation of PMS [209]. This catalyst could be well dispersed in deionized water, effectively
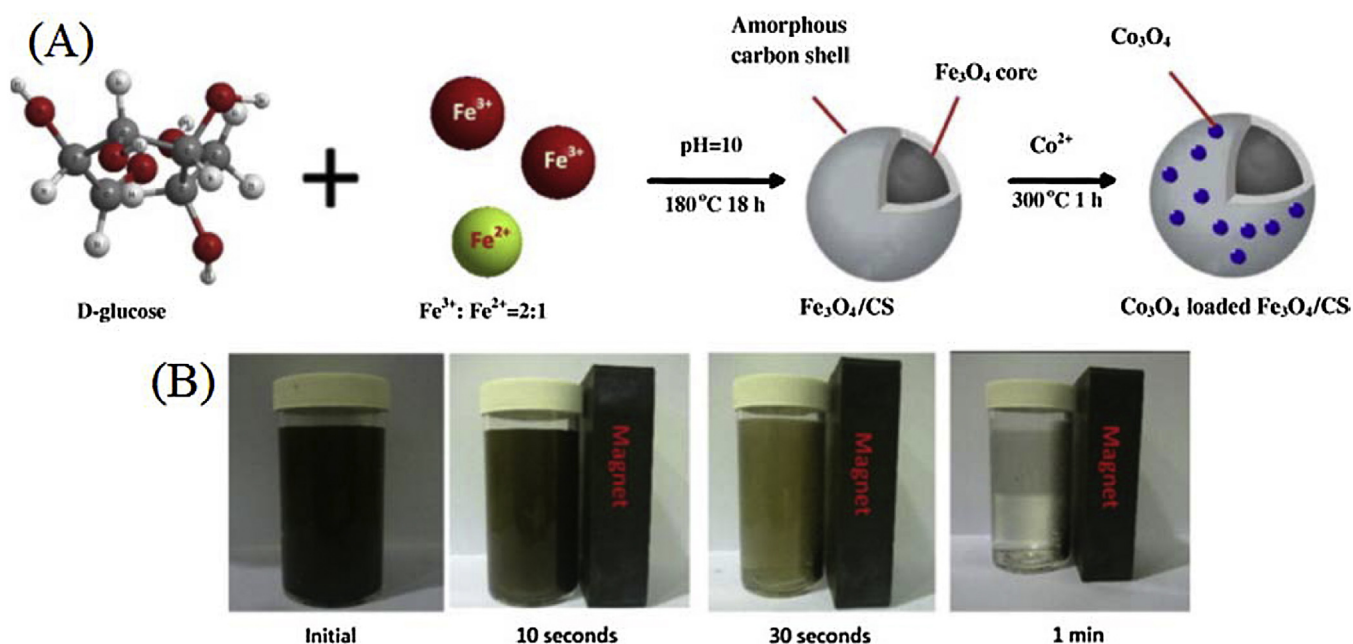
Fig. 7. (A) Preparation procedure and (B) photographs of magnetic separation of Co/MCS.
Source: Reproduced with permission from Ref. [209].

Table 1
Brief summary of synthesis methods for various cobalt-based catalysts.

| Synthesis method	Catalysts	Advantages	Ref.
Thermal decomposition	Co_3O_4	• Facile and efficient	[68,73]
Solvothermal (hydrothermal)	Co_3O_4 $CoFe_2O_4$ Co_3O_4/rGO Co_3O_4/MOF Co/MCS	• Products having tunable morphologies and high crystallinity • Versatile method to prepare various catalysts	[71,103,182,199,209]
Microwave-assisted hydrothermal	Co_3O_4	• High energy efficiency and reproducibility, short reaction time • Capable of separating the nucleation and growth of nanoparticles	[91]
Sol–gel	Co_3O_4 $CoFe_2O_4$ Co/CA	• Low cost, scalable and reproducible • Mild preparation condition	[72,113,126]
Molten salt synthesis	Co_3O_4,	• Avoiding high pressures and surfactants • One-dimensional morphology catalysts	[80]
Co-precipitation	$CoFe_2O_4$	• Compatible with other techniques (e.g. mechanochemical, sonochemical)	[118,119]
Mechanochemical	Co_3O_4 $CoFe_2O_4$	• Simple, low cost and scalable • A solid-state displacement chemical reaction	[79,117]
Solution combustion synthesis	Co/TiO_2, Co/SiO_2 Co/SBA-15	• Highly exothermic, self-sustained and energy-saving • Easy control of chemical compositions	[125,210]
Impregnation	Co/TiO_2 Co/MgO Co/ZSM-5 Co/SBA-15	• Suitable for diverse supported catalysts • Better dispersion	[46,138,154,164]
Ion exchange	Co/ZSM-5	• Lower loading capacity but higher selectivity than impregnation	[50]
Co-condensation	Co/SBA-15 Co/MCM-41	• Simultaneous cobalt incorporation during the synthesis of mesoporous silica • Negligible cobalt leaching	[128,161]
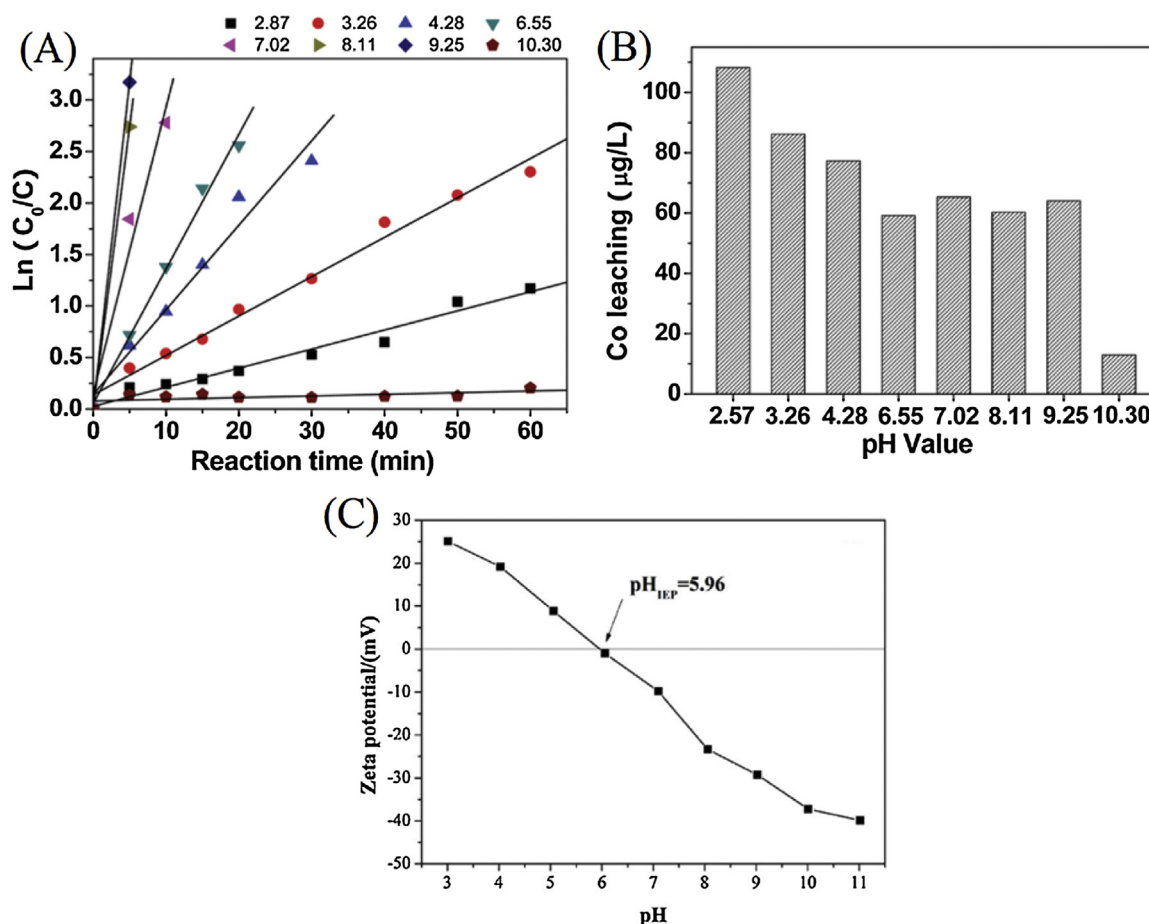
Fig. 8. (A) Kinetic curves and (B) cobalt leaching of heterogeneous PMS activation with Co_3O_4/TiO_2 at different pH ($0.1\,g\,L^{-1}$ catalyst, $0.02\,g\,L^{-1}$ Red-3BS, $0.06\,g\,L^{-1}$ PMS and 298 K). (C) Zeta potential and the IEP of $CoFe_2O_4$.
Source: Reproduced with permission from Refs. [112,211].

separated from water–solid suspensions by an external magnetic field (Fig. 7B), and easily recovered by annealing in air. For easy-reading, the synthesis methods for various cobalt-based catalysts mentioned above have been summarized in Table 1.
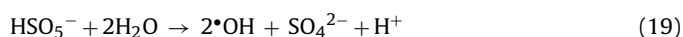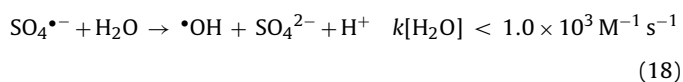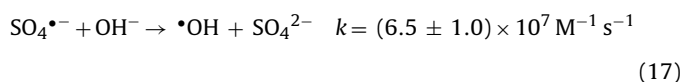
3. Environmental applications

Reaction conditions, such as temperature, pH, dosage of catalysts and PMS, anions and natural organic matter (NOM), affect the performance of heterogeneous Co/PMS systems in the removal of organic compounds. Generally, the catalytic reactions are accelerated with the increases of temperature and dosage of catalysts or PMS, while pH, anions and NOM display complicate influences. Combined with other external energies, the performance of Co/PMS systems would be significantly enhanced. In this section, the influences of solution pH, anions and NOM in heterogeneous Co/PMS suspensions and external energies will be discussed, and the representative environmental applications will also be briefly introduced.

3.1. Influences of reaction conditions

3.1.1. pH

Neutral pH is suitable for organic degradation by Co/PMS system [56], in contrast to excessively acidic or alkaline conditions (Fig. 8A). This phenomenon can be explained in several aspects. The existing form of PMS depends mainly on the solution pH and the second acid dissociation constant ($pK_a = 9.4$). The parent acid,

H_2SO_5, would become the main species instead of HSO_5^- at lower pH [55]. Furthermore, at extremely acidic conditions ($pH \leq 3$), the formation of $CoOH^+$ complex is greatly inhibited, then PMS cannot be effectively activated by cobalt species [14,211]. When solution pH is in the range of 3–9, unlike the limitations of Fenton reaction at higher pH levels, OH^-/H_2O would be oxidized into $^\bullet OH$ by $SO_4^{\bullet-}$ and/or HSO_5^- at a moderate rate (Eqs. (17)–(19)) [212]. The presence of both $SO_4^{\bullet-}$ (dominator) and $^\bullet OH$ maintains a relatively high decontamination efficiency. However, when increasing the solution pH to above 10, $^\bullet OH$ would scavenge $SO_4^{\bullet-}$ and become the dominator, which possesses weaker oxidation capacity than $SO_4^{\bullet-}$ [19]. Simultaneously, cobalt hydroxide complexes would be produced at high pH conditions, resulting in the decreased oxidation potential and catalytic activity [54,56]. Solution pH also affects the stability of cobalt-based catalysts. Evidences have shown that cobalt species, like Co_3O_4 and $Co(OH)_2$ particles, are not stable under acidic conditions [24,213]. A relatively high cobalt leaching at low pH conditions causes possible secondary pollutions and impedes the reuse of the heterogeneous catalysts (Fig. 8B).

$$SO_4^{\bullet-} + OH^- \rightarrow {}^\bullet OH + SO_4^{2-} \quad k = (6.5 \pm 1.0) \times 10^7\,M^{-1}\,s^{-1}$$

$$\text{(17)}$$

$$SO_4^{\bullet-} + H_2O \rightarrow {}^\bullet OH + SO_4^{2-} + H^+ \quad k[H_2O] < 1.0 \times 10^3\,M^{-1}\,s^{-1}$$

$$\text{(18)}$$

$$HSO_5^- + 2H_2O \rightarrow 2^\bullet OH + SO_4^{2-} + H^+ \quad \text{(19)}$$
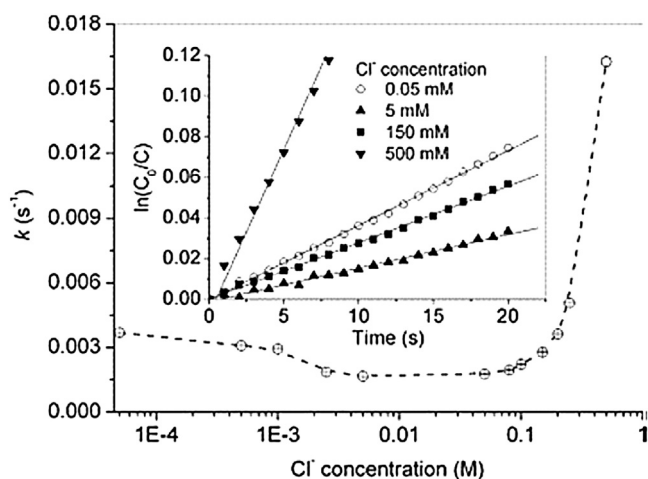
Fig. 9. Effects of Cl^- on Orange II bleaching rate constants (k) in the solution (2.5 mM oxone, 0.1 mM Co^{2+}). Inset: plots of $\ln(C_0/C)$ versus reaction time at various $[Cl^-]$. *Source*: Reproduced with permission from Ref. [214].

The existing form of organic compounds and surface charges of cobalt catalysts (like $CoFe_2O_4$) are closely related to solution pH [56,112]. For example, pK_a of diclofenac (DCF) is 4.15, which means dissociated species (DCF^-) is dominant at pH > 4.15 and nondissociated DCF at pH < 4.15. RhB ($pK_a = 3.7$) has three different species in the aqueous solution at different pH, including cation ($RhBH^+$) and zwitterion ($RhB^{\pm}$) in acidic to neutral solution, and lactone in basic conditions. On the other hand, the isoelectric point (IEP) of $CoFe_2O_4$ is 5.96 (Fig. 8C), indicating that the surface charge of $CoFe_2O_4$ is positive in solution at pH < 5.96. Therefore, by adjusting the solution pH to an appropriate value, target organic molecules would strongly adsorb on the surface of $CoFe_2O_4$ particles by electrostatic attraction, which would favor the decomposition of organic pollutants.

3.1.2. Anions

Anions in Co/PMS systems, such as Cl^-, PO_4^{3-}, HCO_3^-, NO_3^-, would react with active oxidizing species, and influence the performance of the catalytic reactions. Chloride ion (Cl^-), is a pervasive ion in wastewater [214]. Since $SO_4^{\bullet-}$, HSO_5^- and $\bullet OH$ have the potential to oxidize Cl^- to less reactive chlorine or hypochlorous ($E^0_{Cl_2/2Cl^-} = 1.36\,V$ and $E^0_{HOCl/Cl^-} = 1.48\,V$), the presence of Cl^- in Co/PMS systems may dem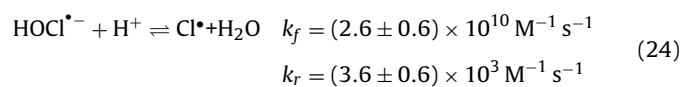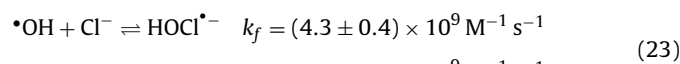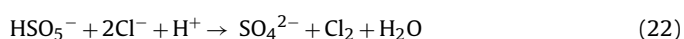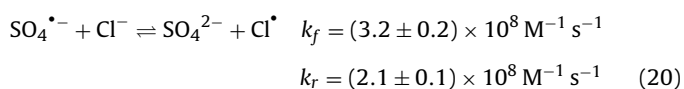onstrate an inhibitory effect, which can be briefly illustrated as Eqs. (20)–(24) [17,47,214,215]. Yuan et al. reported that appreciable amounts of Cl^- in the Co/PMS system would not only reduce the mineralization of azo dye (AO7), but also produce undesirable aromatic chlorinated compounds regardless of cobalt catalysts [17]. However, the inhibitory effect of Cl^- toward dye decolorization only occurs at low concentrations. When $[Cl^-]$ is over a critical concentration, the degradation of dye pollutants (azo or xanthene-type dyes) would be apparently accelerated (Fig. 9) [17,214]. This phenomenon can be understood by that the generated Cl_2 and HOCl in a great amount would rapidly bleach dyes (Eqs. (21) and (22)) and promote the degradation. This was also observed for other halide ions such as Br^- and I^-, but did not happen in H_2O_2 based AOPs probably because Cl^- alone could hardly react with H_2O_2.

$$SO_4^{\bullet-} + Cl^- \rightleftharpoons SO_4^{2-} + Cl^{\bullet} \quad k_f = (3.2 \pm 0.2) \times 10^8\,M^{-1}\,s^{-1}$$
$$k_r = (2.1 \pm 0.1) \times 10^8\,M^{-1}\,s^{-1} \quad (20)$$

$$HSO_5^- + Cl^- \rightleftharpoons SO_4^{2-} + HOCl \quad (21)$$

$$HSO_5^- + 2Cl^- + H^+ \rightarrow SO_4^{2-} + Cl_2 + H_2O \quad (22)$$

$$\bullet OH + Cl^- \rightleftharpoons HOCl^{\bullet-} \quad k_f = (4.3 \pm 0.4) \times 10^9\,M^{-1}\,s^{-1}$$
$$k_r = (6.1 \pm 0.8) \times 10^9\,M^{-1}\,s^{-1} \quad (23)$$

$$HOCl^{\bullet-} + H^+ \rightleftharpoons Cl^{\bullet} + H_2O \quad k_f = (2.6 \pm 0.6) \times 10^{10}\,M^{-1}\,s^{-1}$$
$$k_r = (3.6 \pm 0.6) \times 10^3\,M^{-1}\,s^{-1} \quad (24)$$

$$SO_4^{\bullet-} + CO_3^{2-} \rightarrow CO_3^{\bullet-} + SO_4^{2-} \quad k = 6.1 \times 10^6\,M^{-1}\,s^{-1}$$
$$(pH \geq 11) \quad (25)$$

$$SO_4^{\bullet-} + HCO_3^- \rightarrow HCO_3^{\bullet} + SO_4^{2-} \quad k = 2.8 \times 10^6\,M^{-1}\,s^{-1} \quad (26)$$

$$\bullet OH + HCO_3^- \rightarrow CO_3^{2-} + H_2O \quad k = 8.5 \times 10^6\,M^{-1}\,s^{-1} \quad (27)$$

$$\bullet OH + HPO_4^{2-} \rightarrow HPO_4^{\bullet-} + OH^- \quad k = 1.5 \times 10^5\,M^{-1}\,s^{-1} \quad (28)$$

$$\bullet OH + H_2PO_4^- \rightarrow H_2PO_4^{\bullet} + OH^- \quad k = 2.0 \times 10^4\,M^{-1}\,s^{-1} \quad (29)$$
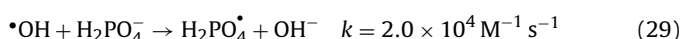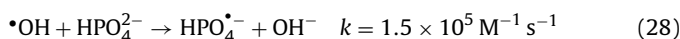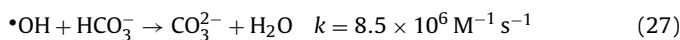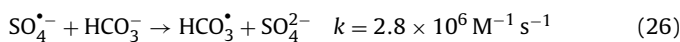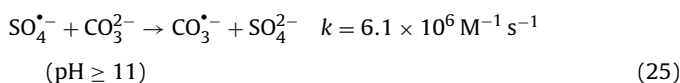
Carbonate/bicarbonate (CO_3^{2-}/HCO_3^-) and phosphate ions (HPO_4^{2-} or $H_2PO_4^-$) have similar influence to quench $SO_4^{\bullet-}$ and/or $\bullet OH$ (Eqs. (25)–(29)) [131,216]. Moreover, phosphate ions have a more apparently abominable effect on the catalysts through chelating reactions, which decreases the active cobalt species on the catalyst surface. Qi et al. revealed that with the increase of phosphate ions, the generation of cobalt/phosphate complex inhibits the performance of CAF degradation both in homogeneous and heterogeneous activations [131].

On the other hand, CO_3^{2-}, HCO_3^-, HPO_4^{2-} were also proven to be capable of activating PMS to generate active species for organics degradation [217]. Other anions, such as nitrate ion (NO_3^-) and perchlorate ion (ClO_4^-), have an unexpected positive effect due to the production of active oxygen during the degradation [47].

3.1.3. Natural organic matter

Natural organic matter (NOM) is a ubiquitous complex constituent in natural waters and soils and would either enhance or inhibit the degradation of organic compounds depending on the concentration and type of NOM [216,218,219]. It has been pointed out that in some cases the reaction of NOM with $SO_4^{\bullet-}$ is far slower than with $\bullet OH$, which means the presence of NOM might have less influence on the performance of SR-AOPs toward target pollutants [220]. Meanwhile, NOM might also stimulate the activation of PMS to generate $SO_4^{\bullet-}$ due to the formation of semiquinone radicals deriving from hydroquinones, quinones and phenols in NOM [219]. However, NOM would also exhibit detrimental effects. NOM usually acts as a scavenger of $SO_4^{\bullet-}$ and $\bullet OH$. According to Yao et al., the degradation efficiency of RhB by $CoMn_2O_4$/PMS decreased from 100% to 48% with the increase of fulvic acid (FA) from 0 to 0.08 g L^{-1} because FA would compete with RhB for reactive radicals [221]. Moreover, phenolic hydroxyl and carboxyl groups of NOM would be adsorbed onto the surface of heterogeneous catalysts and prohibit the contact of PMS and active sites [219]. Thus, in the practical application of heterogeneous Co/PMS system, NOM should be taken into account.

3.2. External energy

Combined with external energy field, including UV–Vis, ultrasound (US), and electrochemistry, the Co/PMS system displays dramatically synergistic enhanced performance.

3.2.1. UV–Vis irradiation

Several studies have shown that the combination of UV–Vis irradiation and Co/PMS systems exhibits a significant enhanced degradation efficiency [54,222–224]. UV light can directly promote the generation of radical species ($SO_4^{\bullet-}$) through the photolysis of
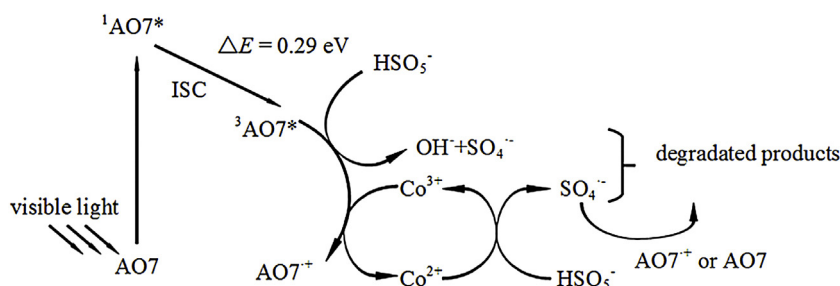
Fig. 10. Proposed reaction mechanism of AO7 degradation in a Vis/Co/PMS system.
Source: Reproduced with permission from Ref. [31].

PMS. When both cobalt species and PMS are present, interaction between them could produce a transition state adduct that is able to absorb UV light [222]. It has been also pointed out that Co^{3+} could convert back to Co^{2+} via photoreduction under UV irradiation [225]. Vis light cannot activate PMS, but the excitation of some target organic molecules would induce a series of chain reactions. Chen et al. reported that in the Vis/Co/PMS system, excited AO7 molecules transfer electrons to PMS or Co^{3+} (Fig. 10), which thus accelerates the decomposition of PMS and promotes catalytic cycle of Co^{2+}/Co^{3+} [31]. Solar driven Co/PMS process seems to be an applicable energy-saving technique [222,223]. Besides UV and Vis light, the range of infrared (IR) light in the sunlight can be utilized to elevate the temperature of the reaction system, so as to facilitate the catalytic reactions.

As mentioned in Section 2.3.1, immobilizing cobalt species on suitable supports (photocatalysts like TiO_2, ZnO) can achieve outstanding degradation performance. This attributes to the interactions between cobalt species and supports, and the simultaneous generation of highly reactive radicals $SO_4^{\bullet-}$ and $^{\bullet}OH$ when irradiated by UV–Vis [53,54,146]. Zhou et al. prepared different cobalt supported titanates, including $ZnTiO_3$, $FeTiO_3$ and $Bi_4Ti_3O_{12}$, and found differences in their photochemical efficiency in phenol removal by PMS activation [124]. $Co/Bi_4Ti_3O_{12}$ showed the best activity because of its higher VB edge (Eq. (30)), while $Co/FeTiO_3$ exhibited the worst activity probably due to the reaction between photoelectrons and surface hydroxyl species, decreasing the production of $CoOH^+$ (Eq. (31)).

$$h_{VB}^+ + SO_4^{2-} \rightarrow SO_4^{\bullet-} \tag{30}$$

$$e_{CB}^- + CoOH^+ \rightarrow (CoOH)^{\bullet} \tag{31}$$

3.2.2. Ultrasonic

During the US irradiation, the tiny gas bubbles in water can form, grow and collapse. The acoustic cavitation is an important phenomenon, where the collapse of cavitation bubbles induces in situ extreme conditions of several thousand degrees and several hundred atmospheres [226]. Then PMS can be directly activated, and $^{\bullet}OH$ can also generate simultaneously, which enhance the degradation efficiency of organics [227]. Guo et al. pointed out that US would accelerate the removal of amoxicillin in the Co_3O_4/PMS system due to direct decomposition of PMS by US irradiation [51]. Cai et al. attributed the enhanced degradation efficiency of Orange II upon US power to the cavitation effects and the assistance in surface cleaning of catalysts by the microstreaming [162]. However, too high US power would not further enhance the degradation efficiency, which was ascribed to the insufficient collapse of the cavitation bubbles.

3.2.3. External electric field

The regeneration of Co^{2+} in catalytic reactions is a key factor for the decontamination efficiency. As mentioned in Section 2.2, Fe^{2+} can spontaneously reduce Co^{3+}. By combined with electrochemistry, Fe^{2+} is electro-regenerated by cathodic reduction of Fe^{3+} (Eq. (6)). Meanwhile, Co^{3+} is directly reduced to Co^{2+} at cathode via Eq. (7) or by Fe^{2+} via Eq. (8). The regeneration of Fe^{2+} and Co^{2+} would enhance the formation of $SO_4^{\bullet-}$ and promote the degradation of organic compounds [210]. Furthermore, as an analog of electro-Fenton process, H_2O_2 would be electrogenerated in situ by the reduction of dissolved oxygen at cathode (Eq. (32)) [4], and Co^{2+} ions have the ability to activate H_2O_2 and generate $^{\bullet}OH$. Cai et al. have applied the electrochemical enhanced Fe-Co/SBA-15/PS system to degrade Orange II [210]. The results showed that the removal efficiency of Orange II and the decomposition of PS increased from 18.2% to 95.6% and 14.9% to 42.3%, respectively, compared to Fe-Co/SBA-15/PS system alone. The dyes could be quickly decolorized in a wide pH range (2–9).

$$O_2 + 2H^+ + 2e^- \rightarrow H_2O_2 \tag{32}$$

3.3. Environmental cleanup

SR-AOP is one of the most promising decontamination technologies due to the generation of reactive oxidizing species $SO_4^{\bullet-}$ and relatively broad application conditions. It has been successfully applied in several environmental cleanup fields including wet air oxidation for wastewater treatment [228], in situ chemical oxidation of contaminated soils and underground water [229], and air pollution control [230]. Up to now, extensive researches on heterogeneous cobalt-catalyzed SR-AOPs have focused on direct chemical oxidation of contaminants in wastewater, such as phenolic contaminants [46,139], dyes [56], herbicides [54,225], plasticizers [180] and medicines [112]. Based on the results of massive experiments, degradation of organic compounds using heterogeneous cobalt-based catalysts for PMS activation follows pseudo zero or first order kinetics. The activation energy (E_a), which is a symbol to tell whether a reaction is easy or hard to occur, can be calculated by the Arrhenius equation (Eq. (33)),

$$\ln(k) = \ln(A) - \frac{E_a}{R}\left(\frac{1}{T}\right) \tag{33}$$

where A is the pre-exponential factor and R is the ideal gas constant. A brief summary of various heterogeneous cobalt-based catalysts in activation of PMS for phenol degradation and the corresponding activation energies are presented in Table 2. It is obvious that the activation energies of Co_3O_4/rGO and $CoFe_2O_4$/rGO systems are relatively lower than others. This is probably related to the large adsorption capacity, the excellent electron transfer ability of rGO and the strong interaction between cobalt species and rGO. The low activation energies of these systems suggest that they are more suitable to be applied for water purification at ambient conditions.

Recently, heterogeneous cobalt catalysts were developed as an oxidation-absorption method to deal with gaseous contaminants (NO_x, SO_2) [233,234]. By conjunction of PMS, oxidation of NO can

Table 2
Activation energies for heterogeneous cobalt-based catalysts with PMS for phenol degradation.

Catalyst	Order of reaction	E_a (kJ/mol)	Ref.
Co_3O_4	First	66.2	[231]
Co/SiO_2	Zero	61.7–75.1	[130]
Co/ZSM-5	Zero	69.7	[50]
Co/SBA-15	Zero	67.4–81.4	[128]
Co/AC	First	59.7	[57]
Co/CA	First	62.9	[126]
Co/CX	First	48.3–62.9	[190]
Co_3O_4/rGO	Zero	26.5	[182]
$CoFe_2O_4$/rGO	First	15.8	[204]
Co/MCS	First	49.1	[209]
Co/fly ash	First	47.0–56.5	[232]
Co/red mud	First	66.3	[58]

achieve a much higher efficiency, and the produced nitrate leaves in the absorption liquid. Sun et al. prepared hybrid Co_3O_4/GO catalyst by wet impregnation method, and used it to oxidize NO [235]. The optimal operation condition was determined as: 6 mM PMS, 0.75 mM Co_3O_4/GO, pH 4.00 and 35 °C. Unlike dissolvable contaminants in water purification, although high temperature would accelerate the activation of PMS, the escape of NO was also promoted, and the total oxidation of NO would decrease.

4. Conclusion and outlook

Generating sulfate radicals by cobalt catalyzed PMS activation has become a promising AOP method for environmental cleanup. Due to the toxicity of excessive cobalt ions, efficient heterogeneous cobalt-based catalysts are urgently demanded. Catalysts containing cobalt species, including Co_3O_4, $CoFe_2O_4$ and cobalt species supported by different solid materials, can be synthesized through various methods and utilized. Heterogeneous Co/PMS systems achieve higher efficiency at neutral pH, and their performance of decontamination can be enhanced when combined with UV–Vis, US and electrochemistry, while anions and NOM have positive or negative influences depending much on their concentrations. The stability and reusability of the heterogeneous cobalt-based catalysts are two important properties that not only ensure a favorable removal of organic compounds with less cobalt leaching, but also make SR-AOPs more economically and environmental friendly. Nevertheless, several aspects of cobalt-based catalysts, heterogeneous Co/PMS systems and their potential applications in practical environmental cleanup deserve further efforts.

(a) It comes to a conclusion that Co_3O_4 and $CoFe_2O_4$ nanoparticles with various morphologies can be obtained through different synthesis routes. However, few studies have been carried out on the mechanism and comparison of the catalytic efficiency of heterogeneous Co/PMS systems with different morphologies of nanocatalysts, which may help enhance the production of reactive oxidative species $SO_4^{\bullet-}$.
(b) Novel synthesis strategies and suitable support materials are necessary to be further studied. More efforts are required to understand the fundamental mechanisms on synergistic effects between supports and active species and their behaviors during the PMS activation cycles, which could be the effective way to realize high catalytic efficiency and simultaneously suppress the leakage of active species.
(c) Homogeneous SR-AOPs have been successfully applied in the in situ chemical oxidation to remove contaminants in polluted soil or underground water. However, heterogeneous catalysts face the difficulty in separation and recovery in open environmental systems. New catalysts and operation techniques, for example, novel magnetically separable catalysts,

heterogeneous catalysts combined with fixed-bed reactors or membrane reactors, are preferable to be developed to expand the application fields of heterogeneous SR-AOPs.
(d) Sulfate leaving in the treated water has a negative effect to the environment, which is a blockage of the wide application of Co/PMS systems. So how to limit the dosage of PMS or improve the efficiency, and how to regenerate PMS in situ are worthy of being investigated. Biological treatment seems to be compatible for the subsequent desulfidation.

Acknowledgements

References

[1] A.R. Ribeiro, O.C. Nunes, M.F.R. Pereira, A.M.T. Silva, Environ. Int. 75 (2015) 33–51.
[2] F. Crapulli, D. Santoro, M.R. Sasges, A.K. Ray, Water Res. 64 (2014) 209–225.
[3] H. Lan, A. Wang, R. Liu, H. Liu, J. Qu, J. Hazard. Mater. 285 (2015) 167–172.
[4] S. Kourdali, A. Badis, A. Boucherit, Ecotoxicol. Environ. Saf. 110 (2014) 110–120.
[5] H. Olvera-Vargas, N. Oturan, E. Brillas, D. Buisson, G. Esposito, M.A. Oturan, Chemosphere 117 (2014) 644–651.
[6] C. Wang, Y. Shih, Purif. Technol. 140 (September) (2015) 6–12.
[7] P. Vaishnave, A. Kumar, R. Ameta, P.B. Punjabi, S.C. Ameta, Arab. J. Chem. 7 (2014) 981–985.
[8] S. Giannakis, S. Papoutsakis, E. Darakas, A. Escalas-Cañellas, C. Pétrier, C. Pulgarin, Ultrason. Sonochem. 22 (2015) 515–526.
[9] G.V. Buxton, C.L. Greenstock, W.P. Helman, A.B. Ross, J. Phys. Chem. Ref. Data 17 (1988) 513–886.
[10] M. Luo, L. Lv, G. Deng, W. Yao, Y. Ruan, X. Li, A. Xu, Appl. Catal. A: Gen. 469 (2014) 198–205.
[11] A. Dhakshinamoorthy, S. Navalon, M. Alvaro, H. Garcia, ChemSusChem 5 (2012) 46–64.
[12] A. De Luca, R.F. Dantas, S. Esplugas, Water Res. 61 (2014) 232–242.
[13] S.A. Messele, O. Soares, J.J.M. Orfao, C. Bengoa, F. Stuber, A. Fortuny, A. Fabregat, J. Font, Catal. Today 240 (2015) 73–79.
[14] P. Neta, R.E. Huie, A.B. Ross, J. Phys. Chem. Ref. Data 17 (1988) 1027–1284.
[15] H. Liu, N. Zhang, Z. Zhu, Chin. Sci. Bull. (Chin. Version) 57 (2012) 3493–3499.
[16] M.G. Antoniou, A.A. de la Cruz, D.D. Dionysiou, Appl. Catal. B: Environ. 96 (2010) 290–298.
[17] R. Yuan, S.N. Ramjaun, Z. Wang, J. Liu, J. Hazard. Mater. 196 (2011) 173–179.
[18] S. Yang, Y. Chen, H. Hu, P. Wang, Y. Liu, M. Wang, Prog. Chem. 20 (2008) 1433–1438.
[19] Y.-F. Huang, Y.-H. Huang, J. Hazard. Mater. 162 (2009) 1211–1216.
[20] E.G. Janzen, Y. Kotake, R.D. Hinton, Free Radic. Biol. Med. 12 (1992) 169–173.
[21] T. Olmez-Hanci, I. Arslan-Alaton, Chem. Eng. J. 224 (2013) 10–16.
[22] M. Banerjee, R.S. Konar, J. Polym. Sci. Polym. Chem. 22 (1984) 1193–1195.
[23] M. Nie, Y. Yang, Z. Zhang, C. Yan, X. Wang, H. Li, W. Dong, Chem. Eng. J. 246 (2014) 373–382.
[24] X. Chen, J. Chen, X. Qiao, D. Wang, X. Cai, Appl. Catal. B: Environ. 80 (2008) 116–121.
[25] Q. Liu, Z. Zheng, X. Yang, X. Luo, J. Zhang, B. Zheng, Environ. Sci. Pollut. Res. 19 (2012) 577–584.
[26] C. Liang, C.J. Bruell, M.C. Marley, K.L. Sperry, Chemosphere 55 (2004) 1213–1223.
[27] E.A. Betterton, M.R. Hoffmann, J. Phys. Chem. 92 (1988) 5962–5965.
[28] K.-C. Huang, R.A. Couttenye, G.E. Hoag, Chemosphere 49 (2002) 413–420.
[29] X. Chen, W. Wang, H. Xiao, C. Hong, F. Zhu, Y. Yao, Z. Xue, Chem. Eng. J. 193–194 (2012) 290–295.
[30] J. Sun, X. Li, J. Feng, X. Tian, Water Res. 43 (2009) 4363–4369.
[31] X. Chen, X. Qiao, D. Wang, J. Lin, J. Chen, Chemosphere 67 (2007) 802–808.
[32] O. Ermer, C. Robke, Helv. Chim. Acta 86 (2003) 2908–2913.
[33] G.P. Anipsitakis, D.D. Dionysiou, Environ. Sci. Technol. 38 (2004) 3705–3712.
[34] G.P. Anipsitakis, D.D. Dionysiou, Environ. Sci. Technol. 37 (2003) 4790–4797.
[35] D.L. Ball, J.O. Edwards, J. Phys. Chem. 62 (1958) 343–345.
[36] S. Tsukada, H. Miki, J.-M. Lin, T. Suzuki, M. Yamada, Anal. Chim. Acta 371 (1998) 163–170.
[37] M. Wang, L. Zhao, M. Liu, J.-M. Lin, Spectrochim. Acta A 66 (2007) 1222–1227.
[38] M. Endo, S. Abe, Y. Deguchi, T. Yotsuyanagi, Talanta 47 (1998) 349–353.
[39] J. Zou, J. Ma, X. Zhang, P. Xie, Chem. Eng. J. 253 (2014) 34–39.
[40] G.A. McLachlan, J.G. Muller, S.E. Rokita, C.J. Burrows, Inorg. Chim. Acta 251 (1996) 193–199.
[41] M. Moradi, F. Ghanbari, J. Water Process Eng. 4 (2014) 67–73.
[42] M. Mahdi Ahmed, S. Barbati, P. Doumenq, S. Chiron, Chem. Eng. J. 197 (2012) 440–447.

[43] Y.-F. Huang, Y.-H. Huang, J. Hazard. Mater. 167 (2009) 418–426.
[44] J. Kim, J.O. Edwards, Inorg. Chim. Acta 235 (1995) 9–13.
[45] P. Shi, X. Dai, H. Zheng, D. Li, W. Yao, C. Hu, Chem. Eng. J. 240 (2014) 264–270.
[46] Q. Yang, H. Choi, D.D. Dionysiou, Appl. Catal. B: Environ. 74 (2007) 170–178.
[47] Y.-H. Huang, Y.-F. Huang, C.-i. Huang, C.-Y. Chen, J. Hazard. Mater. 170 (2009) 1110–1118.
[48] F.J. Rivas, O. Gimeno, T. Borallho, Chem. Eng. J. 192 (2012) 326–333.
[49] D.G. Barceloux, Clin. Toxicol. 37 (1999) 201–216.
[50] P. Shukla, S. Wang, K. Singh, H.M. Ang, M.O. Tadé, Appl. Catal. B: Environ. 99 (2010) 163–169.
[51] W. Guo, S. Su, C. Yi, Z. Ma, Environ. Prog. Sustain. Energy 32 (2013) 193–197.
[52] T.-L. Lai, Y.-L. Lai, C.-C. Lee, Y.-Y. Shu, C.-B. Wang, Catal. Today 131 (2008) 105–110.
[53] J.G. Cabanas-Moreno, Appl. Catal. B: Environ. 77 (2008) 300–307.
[54] K.H. Chan, W. Chu, Water Res. 43 (2009) 2513–2521.
[55] Y. Ren, L. Lin, J. Ma, J. Yang, J. Feng, Z. Fan, Appl. Catal. B: Environ. 165 (2015) 572–578.
[56] S. Su, W. Guo, Y. Leng, C. Yi, Z. Ma, J. Hazard. Mater. 244 (2013) 736–742.
[57] P.R. Shukla, S. Wang, H. Sun, H.M. Ang, M. Tadé, Appl. Catal. B: Environ. 100 (2010) 529–534.
[58] E. Saputra, S. Muhammad, H. Sun, H.M. Ang, M.O. Tadé, S. Wang, Catal. Today 190 (2012) 68–72.
[59] W. Yao, J. Yang, J. Wang, Y. Nuli, J. Electrochem. Soc. 155 (2008) A903–A908.
[60] W. Song, A.S. Poyraz, Y. Meng, Z. Ren, S.-Y. Chen, S.L. Suib, Chem. Mater. 26 (2014) 4629–4639.
[61] A.N. Pour, M. Housaindokht, Catal. Lett. 143 (2013) 1328–1338.
[62] J. Wöllenstein, M. Burgmair, G. Plescher, T. Sulima, J. Hildenbrand, H. Böttner, I. Eisele, Sens. Actuators B: Chem. 93 (2003) 442–448.
[63] C.-W. Tang, C.-B. Wang, S.-H. Chien, Thermochim. Acta 473 (2008) 68–73.
[64] H.-K. Lin, H.-C. Chiu, H.-C. Tsai, S.-H. Chien, C.-B. Wang, Catal. Lett. 88 (2003) 169–174.
[65] C.-B. Wang, H.-K. Lin, C.-W. Tang, Catal. Lett. 94 (2004) 69–74.
[66] G.P. Anipsitakis, E. Stathatos, D.D. Dionysiou, J. Phys. Chem. B 109 (2005) 13052–13055.
[67] Z. Yu, M. Bensimon, D. Laub, L. Kiwi-Minsker, W. Jardim, E. Mielczarski, J. Mielczarski, J. Kiwi, J. Mol. Catal. A: Chem. 272 (2007) 11–19.
[68] S. Farhadi, K. Pourzare, S. Bazgir, J. Alloys Compd. 587 (2014) 632–637.
[69] J. Jiu, Y. Ge, X. Li, L. Nie, Mater. Lett. 54 (2002) 260–263.
[70] J. Mu, L. Zhang, M. Zhao, Y. Wang, J. Mol. Catal. A: Chem. 378 (2013) 30–37.
[71] C. Feng, H. Wang, J. Zhang, W. Hu, Z. Zou, Y. Deng, J. Nanopart. Res. 16 (2014) 2413.
[72] N.N. Binitha, P.V. Suraja, Z. Yaakob, M.R. Resmi, P.P. Silija, J. Sol–Gel Sci. Technol. 53 (2010) 466–469.
[73] D.-S. Wang, T. Xie, Q. Peng, S.-Y. Zhang, J. Chen, Y.-D. Li, Chem. Eur. J. 14 (2008) 2507–2513.
[74] J. Straszko, M. Olszak-Humienik, J. Możejko, J. Therm. Anal. 59 (2000) 935–942.
[75] R.W. Grimes, A.N. Fitch, J. Mater. Chem. 1 (1991) 461.
[76] B. Malecka, E. Drozdz-Ciesla, A. Malecki, J. Therm. Anal. 68 (2002) 819–831.
[77] K. Kalpanadevi, C.R. Sinduja, R. Manimekalai, Aust. J. Chem. 67 (2014) 1671–1674.
[78] H. Yang, Y. Hu, X. Zhang, G. Qiu, Mater. Lett. 58 (2004) 387–389.
[79] M. Ilyas, M. Saeed, Int. J. Chem. React. Eng. 8 (2010).
[80] X. Ke, J. Cao, M. Zheng, Y. Chen, J. Liu, G. Ji, Mater. Lett. 61 (2007) 3901–3903.
[81] Y. Ni, X. Ge, Z. Zhang, H. Liu, Z. Zhu, Q. Ye, Mater. Res. Bull. 36 (2001) 2383–2387.
[82] L. Cui, J. Li, X.-G. Zhang, J. Appl. Electrochem. 39 (2009) 1871–1876.
[83] X. Liu, R. Yi, N. Zhang, R. Shi, X. Li, G. Qiu, J. Chem. Asian J. 3 (2008) 732–738.
[84] S.C. Petitto, E.M. Marsh, G.A. Carson, M.A. Langell, J. Mol. Catal. A: Chem. 281 (2008) 49–58.
[85] X.-Y. Yu, Q.-Q. Meng, T. Luo, Y. Jia, B. Sun, Q.-X. Li, J.-H. Liu, X.-J. Huang, Sci. Rep. 3 (2013) 2886.
[86] Y. Li, W.J. Shen, Chem. Soc. Rev. 43 (2014) 1543–1574.
[87] L. Hu, K. Sun, Q. Peng, B. Xu, Y. Li, Nano Res. 3 (2010) 363–368.
[88] T.A. Dankovich, Environ. Sci. Nano 1 (2014) 367–378.
[89] H.A. Elazab, S. Moussa, B.F. Gupton, M.S. El-Shall, J. Nanopart. Res. 16 (2014) 2477.
[90] W.-W. Wang, Y.-J. Zhu, Mater. Res. Bull. 40 (2005) 1929–1935.
[91] T.A. Mulinari, F.A. La Porta, J. Andres, M. Cilense, J.A. Varela, E. Longo, CrystEngComm 15 (2013) 7443–7449.
[92] S. Chen, Y. Zhao, B. Sun, Z. Ao, X. Xie, Y. Wei, G. Wang, ACS Appl. Mater. Interfaces 7 (2015) 3306–3313.
[93] H. Shao, Y. Huang, H. Lee, Y.J. Suh, C.O. Kim, J. Magn. Magn. Mater. 304 (2006) e28–e30.
[94] M. Salavati-Niasari, F. Davar, M. Mazaheri, M. Shaterian, J. Magn. Magn. Mater. 320 (2008) 575–578.
[95] M. Salavati-Niasari, Z. Fereshteh, F. Davar, Polyhedron 28 (2009) 1065–1068.
[96] L. Zhuo, J. Xu, H. Miao, F. Wang, X. Li, Appl. Catal. A: Gen. 292 (2005) 223–228.
[97] L. Cao, M. Lu, H.-L. Li, J. Electrochem. Soc. 152 (2005) A871–A875.
[98] Y. Zhang, Y. Liu, S. Fu, F. Guo, Y. Qian, Mater. Chem. Phys. 104 (2007) 166–171.
[99] S. Elhag, Z. Ibupoto, O. Nour, M. Willander, Materials 8 (2014) 149–161.
[100] L. Ren, P. Wang, Y. Han, C. Hu, B. Wei, Chem. Phys. Lett. 476 (2009) 78–83.
[101] R. Xu, H.C. Zeng, J. Phys. Chem. B 107 (2003) 12643–12649.
[102] A.-M. Cao, J.-S. Hu, H.-P. Liang, W.-G. Song, L.-J. Wan, X.-L. He, X.-G. Gao, S.-H. Xia, J. Phys. Chem. B 110 (2006) 15858–15863.
[103] E. Pervaiz, I.H. Gul, H. Anwar, J. Supercond. Novel Magn. 26 (2013) 415–424.
[104] A. Hannour, D. Vincent, F. Kahiouche, A. Tchangoulian, S. Neveu, V. Dupuis, J. Magn. Magn. Mater. 353 (2014) 29–33.
[105] J. Ding, Y.J. Chen, Y. Shi, S. Wang, Appl. Phys. Lett. 77 (2000) 3621–3623.
[106] M. Bonini, A. Wiedenmann, P. Baglioni, Physica A 339 (2004) 86–91.
[107] E. Fantechi, C. Innocenti, M. Zanardelli, M. Fittipaldi, E. Falvo, M. Carbo, V. Shullani, L.D. Mannelli, C. Ghelardini, A.M. Ferretti, A. Ponti, C. Sangregorio, P. Ceci, ACS Nano 8 (2014) 4705–4719.
[108] E. Cespedes, J.M. Byrne, N. Farrow, S. Moise, V.S. Coker, M. Bencsik, J.R. Lloyd, N.D. Telling, Nanoscale 6 (2014) 12958–12970.
[109] Q. Yang, H. Choi, S.R. Al-Abed, D.D. Dionysiou, Appl. Catal. B: Environ. 88 (2009) 462–469.
[110] S.J. Kim, S.W. Lee, S.Y. An, C.S. Kim, J. Magn. Magn. Mater. 215 (2000) 210–212.
[111] F. Sadri, A. Ramazani, A. Massoudi, M. Khoobi, V. Azizkhani, R. Tarasi, L. Dolat-yari, B.-K. Min, Bull. Korean Chem. Soc. 35 (2014) 2029–2032.
[112] J. Deng, Y. Shao, N. Gao, C. Tan, S. Zhou, X. Hu, J. Hazard. Mater. 262 (2013) 836–844.
[113] C. Cannas, A. Ardu, D. Peddis, C. Sangregorio, G. Piccaluga, A. Musinu, J. Colloid Interface Sci. 343 (2010) 415–422.
[114] B.G. Toksha, S.E. Shirsath, S.M. Patange, K.M. Jadhav, Solid State Commun. 147 (2008) 479–483.
[115] P. Kuruva, S. Matteppanavar, S. Srinath, T. Thomas, IEEE Trans. Magn. 50 (2014) 8.
[116] D. Gherca, A. Pui, N. Cornei, A. Cojocariu, V. Nica, O. Caltun, J. Magn. Magn. Mater. 324 (2012) 3906–3911.
[117] E. Manova, B. Kunev, D. Paneva, I. Mitov, L. Petrov, C. Estournès, C. D'Orléan, J.-L. Rehspringer, M. Kurmoo, Chem. Mater. 16 (2004) 5689–5696.
[118] H. Yang, X. Zhang, A. Tang, G. Qiu, Chem. Lett. 33 (2004) 826–827.
[119] K.K. Senapati, C. Borgohain, P. Phukan, J. Mol. Catal. A: Chem. 339 (2011) 24–31.
[120] S. Yanez-Vilar, M. Sanchez-Andujar, C. Gomez-Aguirre, J. Mira, M.A. Senaris-Rodriguez, S. Castro-Garcia, J. Solid State Chem. 182 (2009) 2685–2690.
[121] S. Feng, G. Li, in: R. Xu, W. Pang, Q. Huo (Eds.), Modern Inorganic Synthetic Chemistry, Elsevier, Amsterdam, 2011, pp. 63–95.
[122] Q. Chen, F. Ji, Q. Guo, J. Fan, X. Xu, J. Environ. Sci. 26 (2014) 2440–2450.
[123] W. Zhang, H.L. Tay, S.S. Lim, Y. Wang, Z. Zhong, R. Xu, Appl. Catal. B: Environ. 95 (2010) 93–99.
[124] G. Zhou, H. Sun, S. Wang, H. Ming Ang, M.O. Tadé, Sep. Purif. Technol. 80 (2011) 626–634.
[125] H. Sun, H. Liang, G. Zhou, S. Wang, J. Colloid Interface Sci. 394 (2013) 394–400.
[126] Y. Hardjono, H. Sun, H. Tian, C.E. Buckley, S. Wang, Chem. Eng. J. 174 (2011) 376–382.
[127] Y. Yao, C. Xu, S. Miao, H. Sun, S. Wang, J. Colloid Interface Sci. 402 (2013) 230–236.
[128] P. Shukla, H. Sun, S. Wang, H.M. Ang, M.O. Tadé, Catal. Today 175 (2011) 380–385.
[129] Z. Chen, S. Chen, Y. Li, X. Si, J. Huang, S. Massey, G. Chen, Mater. Res. Bull. 57 (2014) 170–176.
[130] P. Shukla, H. Sun, S. Wang, H.M. Ang, M.O. Tade, Purif. Technol. 77 (September) (2011) 230–236.
[131] F. Qi, W. Chu, B. Xu, Chem. Eng. J. 235 (2014) 10–18.
[132] A.S. Mukasyan, P. Epstein, P. Dinka, Proc. Combust. Inst. 31 (2007) 1789–1795.
[133] H. Liang, Y.Y. Ting, H. Sun, H.M. Ang, M.O. Tadé, S. Wang, J. Colloid Interface Sci. 372 (2012) 58–62.
[134] G.K. Reddy, G. Thrimurthulu, B.M. Reddy, Catal. Surv. Asia 13 (2009) 237–255.
[135] U. Zavyalova, P. Scholz, B. Ondruschka, Appl. Catal. A: Gen. 323 (2007) 226–233.
[136] A. Bronson, G.S. Pierre, Metall. Trans. B 12 (1981) 729–731.
[137] L. Hu, F. Yang, W. Lu, Y. Hao, H. Yuan, Appl. Catal. B: Environ. 134 (2013) 7–18.
[138] M. Stoyanova, I. Slavova, S. Christoskova, V. Ivanova, Appl. Catal. A: Gen. 476 (2014) 121–132.
[139] L. Hu, X. Yang, S. Dang, Appl. Catal. B: Environ. 102 (2011) 19–26.
[140] F. Ji, C. Li, L. Deng, Chem. Eng. J. 178 (2011) 239–243.
[141] E. Saputra, S. Muhammad, H. Sun, A. Patel, P. Shukla, Z.H. Zhu, S. Wang, Catal. Commun. 26 (2012) 144–148.
[142] S. Muhammad, P.R. Shukla, M.O. Tadé, S. Wang, J. Hazard. Mater. 215–216 (2012) 183–190.
[143] H. Liang, H. Sun, A. Patel, P. Shukla, Z.H. Zhu, S. Wang, Appl. Catal. B: Environ. 127 (2012) 330–335.
[144] M.S. Wrighton, Acc. Chem. Res. 12 (1979) 303–310.
[145] P. Sathishkumar, N. Pugazhenthiran, R.V. Mangalaraja, A.M. Asiri, S. Anandan, J. Hazard. Mater. 252–253 (2013) 171–179.
[146] Q. Chen, F. Ji, T. Liu, P. Yan, W. Guan, X. Xu, Chem. Eng. J. 229 (2013) 57–65.
[147] P. Sathishkumar, R.V. Mangalaraja, S. Anandan, M. Ashokkumar, Chem. Eng. J. 220 (2013) 302–310.
[148] S. Muhammad, E. Saputra, H. Sun, H.M. Ang, M.O. Tadé, S. Wang, Water Air Soil Pollut. 224 (2013) 1–9.
[149] A.A. Verberckmoes, B.M. Weckhuysen, R.A. Schoonheydt, Microporous Mesoporous Mater. 22 (1998) 165–178.
[150] J.C. Kim, S. Lee, K. Cho, K. Na, C. Lee, R. Ryoo, ACS Catal. 4 (2014) 3919–3927.
[151] D. Zhou, B. Tang, X.-H. Lu, X.-L. Wei, K. Li, Q.-H. Xia, Catal. Commun. 45 (2014) 124–128.
[152] M. Mofarahi, F. Gholipour, Microporous Mesoporous Mater. 200 (2014) 1–10.
[153] K. Góra-Marek, B. Gil, M. Śliwa, J. Datka, Appl. Catal. A: Gen. 330 (2007) 33–42.
[154] L.B. Pierella, C. Saux, S.C. Caglieri, H.R. Bertorello, P.G. Bercoff, Appl. Catal. A: Gen. 347 (2008) 55–61.

[155] C.T. Kresge, M.E. Leonowicz, W.J. Roth, J.C. Vartuli, J.S. Beck, Nature 359 (1992) 710–712.
[156] A.Y. Khodakov, V.L. Zholobenko, R. Bechara, D. Durand, Microporous Mesoporous Mater. 79 (2005) 29–39.
[157] D.J. Kim, B.C. Dunn, P. Cole, G. Turpin, R.D. Ernst, R.J. Pugmire, M. Kang, J.M. Kim, E.M. Eyring, Chem. Commun. (2005) 1462–1464.
[158] X.Q. Wang, H.L. Ge, H.X. Jin, Y.J. Cui, Microporous Mesoporous Mater. 86 (2005) 335–340.
[159] M. Colilla, F. Balas, M. Manzano, M. Vallet-Regí, Chem. Mater. 19 (2007) 3099–3101.
[160] Y. Ling, M. Long, P. Hu, Y. Chen, J. Huang, J. Hazard. Mater. 264 (2014) 195–202.
[161] F. Qi, W. Chu, B. Xu, Appl. Catal. B: Environ. 134–135 (2013) 324–332.
[162] C. Cai, H. Zhang, X. Zhong, L. Hou, J. Hazard. Mater. 283 (2015) 70–79.
[163] X. Zhong, J. Barbier, D. Duprez, H. Zhang, S. Royer, Appl. Catal. B: Environ. 121 (2012) 123–134.
[164] Y. Wang, M. Noguchi, Y. Takahashi, Y. Ohtsuka, Catal. Today 68 (2001) 3–9.
[165] J. van der Meer, I. Bardez, F. Bart, P.-A. Albouy, G. Wallez, A. Davidson, Microporous Mesoporous Mater. 118 (2009) 183–188.
[166] J. van der Meer, I. Bardez-Giboire, C. Mercier, B. Revel, A. Davidson, R. Denoyel, J. Phys. Chem. C 114 (2010) 3507–3515.
[167] M. Xia, M. Long, Y. Yang, C. Chen, W. Cai, B. Zhou, Appl. Catal. B: Environ. 110 (2011) 118–125.
[168] J. Zhang, X. Shao, C. Shi, S. Yang, Chem. Eng. J. 232 (2013) 259–265.
[169] J.C. Xu, P.H. Xin, Y.B. Han, P.F. Wang, H.X. Jin, D.F. Jin, X.L. Peng, B. Hong, J. Li, H.L. Ge, Z.W. Zhu, X.Q. Wang, J. Alloys Compd. 617 (2014) 622–626.
[170] W. Lu, W. Chen, N. Li, M. Xu, Y. Yao, Appl. Catal. B: Environ. 87 (2009) 146–151.
[171] Z. Huang, H. Bao, Y. Yao, W. Lu, W. Chen, Appl. Catal. B: Environ. 154–155 (2014) 36–43.
[172] L. Dai, Acc. Chem. Res. 46 (2013) 31–42.
[173] X. Wan, Y. Huang, Y. Chen, Acc. Chem. Res. 45 (2012) 598–607.
[174] X. Cao, Q. He, W. Shi, B. Li, Z. Zeng, Y. Shi, Q. Yan, H. Zhang, Small 7 (2011) 1199–1202.
[175] P. Shi, R. Su, F. Wan, M. Zhu, D. Li, S. Xu, Appl. Catal. B: Environ. 123–124 (2012) 265–272.
[176] S.-Y. Wu, J.-J. Ho, J. Phys. Chem. C 118 (2014) 26764–26771.
[177] M. Long, Y. Qin, C. Chen, X. Guo, B. Tan, W. Cai, J. Phys. Chem. C 117 (2013) 16734–16741.
[178] Y. Xiao, X. Li, J. Zai, K. Wang, Y. Gong, B. Li, Q. Han, X. Qian, Nano-Micro Lett. 6 (2014) 307–315.
[179] Y. Qin, M. Long, B. Tan, B. Zhou, Nano-Micro Lett. 6 (2014) 125–135.
[180] L.J. Xu, W. Chu, L. Gan, Chem. Eng. J. 263 (2015) 435–443.
[181] P. Shi, R. Su, S. Zhu, M. Zhu, D. Li, S. Xu, J. Hazard. Mater. 229 (2012) 331–339.
[182] Y. Yao, Z. Yang, H. Sun, S. Wang, Ind. Eng. Chem. Res. 51 (2012) 14958–14965.
[183] L. Wan, M. Long, D. Zhou, L. Zhang, W. Cai, Nano-Micro Lett. 4 (2012) 90–97.
[184] J. Zhou, H. Song, L. Ma, X. Chen, RSC Adv. 1 (2011) 782–791.
[185] H. Sun, S. Liu, G. Zhou, H.M. Ang, M.O. Tadé, S. Wang, ACS Appl. Mater. Interfaces 4 (2012) 5466–5471.
[186] W. Peng, S. Liu, H. Sun, Y. Yao, L. Zhi, S. Wang, J. Mater. Chem. A 1 (2013) 5854.
[187] D. Fairén-Jiménez, F. Carrasco-Marín, C. Moreno-Castilla, Carbon 44 (2006) 2301–2307.
[188] J. Wang, M.W. Ellsworth, in: Y. Obeng, S. DeGendt, P. Srinivasan, D. Misra, H. Iwai, Z. Karim, D.W. Hess, H. Grebel (Eds.), Graphene and Emerging Materials for Post-CMOS Applications, Electrochemical Society Inc., Pennington, 2009, pp. 241–247.
[189] X.L. Wu, T. Wen, H.L. Guo, S. Yang, X. Wang, A.W. Xu, ACS Nano 7 (2013) 3589–3597.
[190] H. Sun, H. Tian, Y. Hardjono, C.E. Buckley, S. Wang, Catal. Today 186 (2012) 63–68.
[191] S. Hermes, F. Schroder, S. Amirjalayer, R. Schmid, R.A. Fischer, J. Mater. Chem. 16 (2006) 2464–2472.
[192] S. Huh, H.-T. Chen, J.W. Wiench, M. Pruski, V.S.Y. Lin, J. Am. Chem. Soc. 126 (2004) 1010–1011.
[193] T. Uemura, K. Kitagawa, S. Horike, T. Kawamura, S. Kitagawa, M. Mizuno, K. Endo, Chem. Commun. (2005) 5968–5970.
[194] C. Petit, J. Burress, T.J. Bandosz, Carbon 49 (2011) 563–572.
[195] N.L. Rosi, J. Eckert, M. Eddaoudi, D.T. Vodak, J. Kim, M. O'Keeffe, O.M. Yaghi, Science 300 (2003) 1127–1129.
[196] T. Duren, R.Q. Snurr, J. Phys. Chem. B 108 (2004) 15703–15708.
[197] P. Horcajada, C. Serre, M. Vallet-Regi, M. Sebban, F. Taulelle, G. Ferey, Angew. Chem. Int. Ed. 45 (2006) 5974–5978.
[198] K.-Y. Andrew Lin, H.-A. Chang, J. Taiwan Inst. Chem. Eng. 53 (2015) 40–45.
[199] T. Zeng, X. Zhang, S. Wang, H. Niu, Y. Cai, Environ. Sci. Technol. 49 (2015) 2350–2357.
[200] J.-K. Sun, Q. Xu, Chem. Commun. 50 (2014) 13502–13505.
[201] K.-Y. Andrew Lin, F.-K. Hsu, W.-D. Lee, J. Mater. Chem. A 3 (2015) 9480–9490.
[202] F.-X. Qin, S.-Y. Jia, Y. Liu, X. Han, H.-T. Ren, W.-W. Zhang, J.-W. Hou, S.-H. Wu, Mater. Lett. 101 (2013) 93–95.
[203] Q. Song, Z.J. Zhang, J. Am. Chem. Soc. 126 (2004) 6164–6168.
[204] Y. Yao, Z. Yang, D. Zhang, W. Peng, H. Sun, S. Wang, Ind. Eng. Chem. Res. 51 (2012) 6044–6051.
[205] A.R.B. Suganthi, R.J. Usha, P. Sagayaraj, Spectrosc. Lett. 48 (2015) 213–216.
[206] X.F. Zheng, Q. Lian, J. Dispers. Sci. Technol. 36 (2015) 245–251.
[207] X. An, J.C. Yu, RSC Adv. 1 (2011) 1426–1434.
[208] K. Ali, A.K. Sarfraz, A. Ali, A. Mumtaz, S.K. Hasanain, J. Magn. Magn. Mater. 369 (2014) 81–85.
[209] Y.X. Wang, H.Q. Sun, H.M. Ang, M.O. Tade, S.B. Wang, Chem. Eng. J. 245 (2014) 1–9.
[210] C. Cai, H. Zhang, X. Zhong, L. Hou, Water Res. 66 (2014) 473–485.
[211] Y. Zhu, S. Chen, X. Quan, Y. Zhang, RSC Adv. 3 (2013) 520–525.
[212] Z. Yu, W. Wang, L. Song, L. Lu, Z. Wang, X. Jiang, C. Dong, R. Qiu, Chem. Eng. J. 234 (2013) 475–483.
[213] J. Li, Y. Yi, P. Shi, Q. Wang, D.X. Li, H. Asif, M. Yang, Acta Phys. – Chim. Sin. 30 (2014) 1720–1726.
[214] Z. Wang, R. Yuan, Y. Guo, L. Xu, J. Liu, J. Hazard. Mater. 190 (2011) 1083–1087.
[215] P. Wang, S. Yang, L. Shan, R. Niu, X. Shao, J. Environ. Sci. 23 (2011) 1799–1807.
[216] Y. Ji, C. Dong, D. Kong, J. Lu, J. Hazard. Mater. 285 (2015) 491–500.
[217] S. Yang, P. Wang, X. Yang, L. Shan, W. Zhang, X. Shao, R. Niu, J. Hazard. Mater. 179 (2010) 552–558.
[218] M. Drosos, M.J. Ren, F.H. Frimmel, Appl. Catal. B: Environ. 165 (2015) 328–334.
[219] Y.-H. Guan, J. Ma, Y.-M. Ren, Y.-L. Liu, J.-Y. Xiao, L.-q. Lin, C. Zhang, Water Res. 47 (2013) 5431–5438.
[220] X. He, A.A. de la Cruz, K.E. O'Shea, D.D. Dionysiou, Water Res. 63 (2014) 168–178.
[221] Y. Yao, Y. Cai, G. Wu, F. Wei, X. Li, H. Chen, S. Wang, J. Hazard. Mater. 296 (2015) 128–137.
[222] E.R. Bandala, M.A. Peláez, D.D. Dionysiou, S. Gelover, J. Garcia, D. Macías, J. Photochem. Photobiol. A: Chem. 186 (2007) 357–363.
[223] E.R. Bandala, M.A. Peláez, M.J. Salgado, L. Torres, J. Hazard. Mater. 151 (2008) 578–584.
[224] E.R. Bandala, L. Brito, M. Pelaez, Desalination 245 (2009) 135–145.
[225] W. Chu, W.K. Choy, C.Y. Kwan, J. Agric. Food Chem. 55 (2007) 5708–5713.
[226] W.-S. Chen, Y.-C. Su, Ultrason. Sonochem. 19 (2012) 921–927.
[227] L. Hou, L. Zhang, X. Xue, Purif. Technol. 84 (September) (2012) 147–152.
[228] F.J. Rivas, F.J. Beltrán, F. Carvalho, P.M. Alvarez, Ind. Eng. Chem. Res. 44 (2005) 749–758.
[229] M. Usman, P. Faure, C. Ruby, K. Hanna, Chemosphere 87 (2012) 234–240.
[230] N.E. Khan, Y.G. Adewuyi, Ind. Eng. Chem. Res. 49 (2010) 8749–8760.
[231] E. Saputra, S. Muhammad, H.Q. Sun, H.M. Ang, M.O. Tade, S.B. Wang, J. Colloid Interface Sci. 407 (2013) 467–473.
[232] S. Muhammad, E. Saputra, H.Q. Sun, J.D. Izidoro, D.A. Fungaro, H.M. Ang, M.O. Tade, S.B. Wang, RSC Adv. 2 (2012) 5645–5650.
[233] Y. Huang, D. Gao, Z. Tong, J. Zhang, H. Luo, J. Nat. Gas Chem. 18 (2009) 421–428.
[234] M.F. Irfan, J.H. Goo, S.D. Kim, Appl. Catal. B: Environ. 78 (2008) 267–274.
[235] X. Sun, M. Yang, X. Shao, D. Li, Environ. Sci. Technol. 37 (2014), 125–128 + 143 (in Chinese).